AMBIPOLAR ELECTRIC FIELDS AND TURBULENCE STUDIES IN THE WISCONSIN LEVITATED TOROIDAL OCTUPOLE

BY

CHARLES JESSE ARMENTROUT

A thesis submitted in partial fulfillment of the requirements for the degree of

DOCTOR OF PHILOSOPHY

(Physics)

at the

UNIVERSITY OF WISCONSIN-MADISON

1977

ABSTRACT

AMBIPOLAR ELECTRIC FIELDS AND TURBULENCE STUDIES

IN THE WISCONSIN LEVITATED TOROIDAL OCTUPOLE

Charles Jesse Armentrout

Under the Direction of Professor D. W. Kerst

Detailed studies of hot ion plasmas ($T_i > T_e$) in the poloidal field octupole show that the ambipolar electric field which is perpendicular to the flux surfaces is well explained by the observed properties of the microturbulence structures in the plasma.

The radial electric fields decay at the rate which is the sum of the decay rates of the ion temperature and the inverse density scale length. The potential in the plasma is related to the density by the ambipolar relationship with the diffusion and mobility coefficients treated as unrelated phenomenological parameters. This relationship between the electric field, the ion temperature, and the density is seen to hold for a variety of operating conditions. It is shown that ambipolarity need not require vector equality between the ion and electron fluxes at every point in space and a particle flux imbalance may well exist. This imbalance has important implications for the experimental measurement of various quantities.

The turbulence structure has been measured by correlation techniques which are carefully described. In these experiments, signals were studied which are aperiodic in time and space, short lived compared to the decay times of the bulk plasma parameters, short ranged

compared to the machine size, and are therefore classified as micro-turbulence structures. The resulting spatial and temporal correlation functions (CFs) are well fitted to a Gaussian function and the associated correlation lengths or times are the half width at half maximum of the CFs. The correlation length is measured to be the ion gyro radius for the hot hydrogen plasma and somewhat less for the helium plasma. The measured correlation time is comparable to the disassembly time of such a cell from the influence of the magnetic gradient and curvature drifts.

The observations suggest a model in which the cell-like structures are composed from the electron distribution. Electron diffusion results from the vortex motion of an electron in the cell field until the cell decorrelates. The resulting electron mobility coefficient is zero. The ion-cell interaction results in both diffusion and mobility coefficients. This model explains the observed ambipolar electric field and gives an estimate of the diffusion coefficient which is within a factor of four of the previously measured value.

The amplitude of the cells is larger than predicted for spontaneous random thermal fluctuations. Suggestions have been made that such cells could be driven in amplitude by long wavelength coherent oscillations. Such waves are always seen to coexist with the turbulence structures and are identified as hot ion flute modes.

Donald M. Kerr,

ACKNOWLEDGEMENTS

The author would like to express his appreciation to the many people who have helped in this work and in particular to Dr. D. W. Kerst for his patient support of the research project reported here.

I would like to especially thank Dr. K. R. Symon for the many useful discussions which guided my work and my analysis on the proper path. I would also like to thank Dr. G. A. Emmert for his interest, especially in the basic problems involved in the analysis of plasma turbulence.

The many helpful discussions with Dr. J. R. Greenwood on the observed diffusion processes in the octupole are greatly appreciated. His development of the computer interface system made this work feasible. I would also like to express my appreciation to Mike Zarnstorff for the development of the REBEL/BASIC software used to acquire and analyze the majority of the data presented below. The many discussions with Jim and Mike about the care and feeding of an acquisition system have been quite enlightening.

I would in particular like to thank Paul Nonn for his invaluable aid in the design and initial construction of the special probes and circuits used. I also wish to give special thanks to John Laufenberg for advice and aid in the daily effort to keep the machine and the computer running, and for aid in the construction and development of most of the electronic circuits employed.

TABLE OF CONTENTS

CHAPTER II: DATA ACQUISITION AND ANALYSIS TECHNIQUES

CHAPTER III: BULK PROPERTIES OF THE PLASMA

CHAPTER IV: TURBULENCE STUDIES

CHAPTER IV: TURBULENCE STUDIES (cont.)

CHAPTER V: COHERENT FLUCTUATIONS IN THE HOT ION PLASMA

CHAPTER I: THE WISCONSIN LEVITATED TOROIDAL OCTUPOLE

A: Description Of The Octupole

(i) Mechanical And Electrical Construction

The Wisconsin levitated toroidal octupole is shown in the diagram of Figure 1. The machine is composed of four current carrying rings inside a 9 cubic meter toroidal vacuum chamber of noncircular cross section and is constructed of high conductivity aluminum. It measures 2.5 meters between the top lid of the chamber and the laboratory floor and 4 meters in outside diameter. The four internal rings shape the magnetic field into an octupole pattern which is modified by the presence of the conductive walls. The current in the rings is inductively driven by the iron core transformer, the rings being four single turn secondary windings linking the core in parallel.

The device is the second generation successor of the smaller octupole located in the Wisconsin physics department. It was designed partly to discover what portion of the plasma loss is due to the supports which hold the rings in position. The machine was built to do this using two major modifications of the design of the first generation device. The outer and inner walls are indented to enclose the rings partially. This allows the rings to be positioned so that the net vertical and horizontal forces on them due to the wall currents are zero. Because of this free-force positioning, the rings merely rest on their supports which need hold them only against gravity. During the field pulse, the supports may be removed from ring contact for a total of about sixty milliseconds to keep the rings from falling more than a

Figure I 1

The Wisconsin Levitated Toroidal Octupole

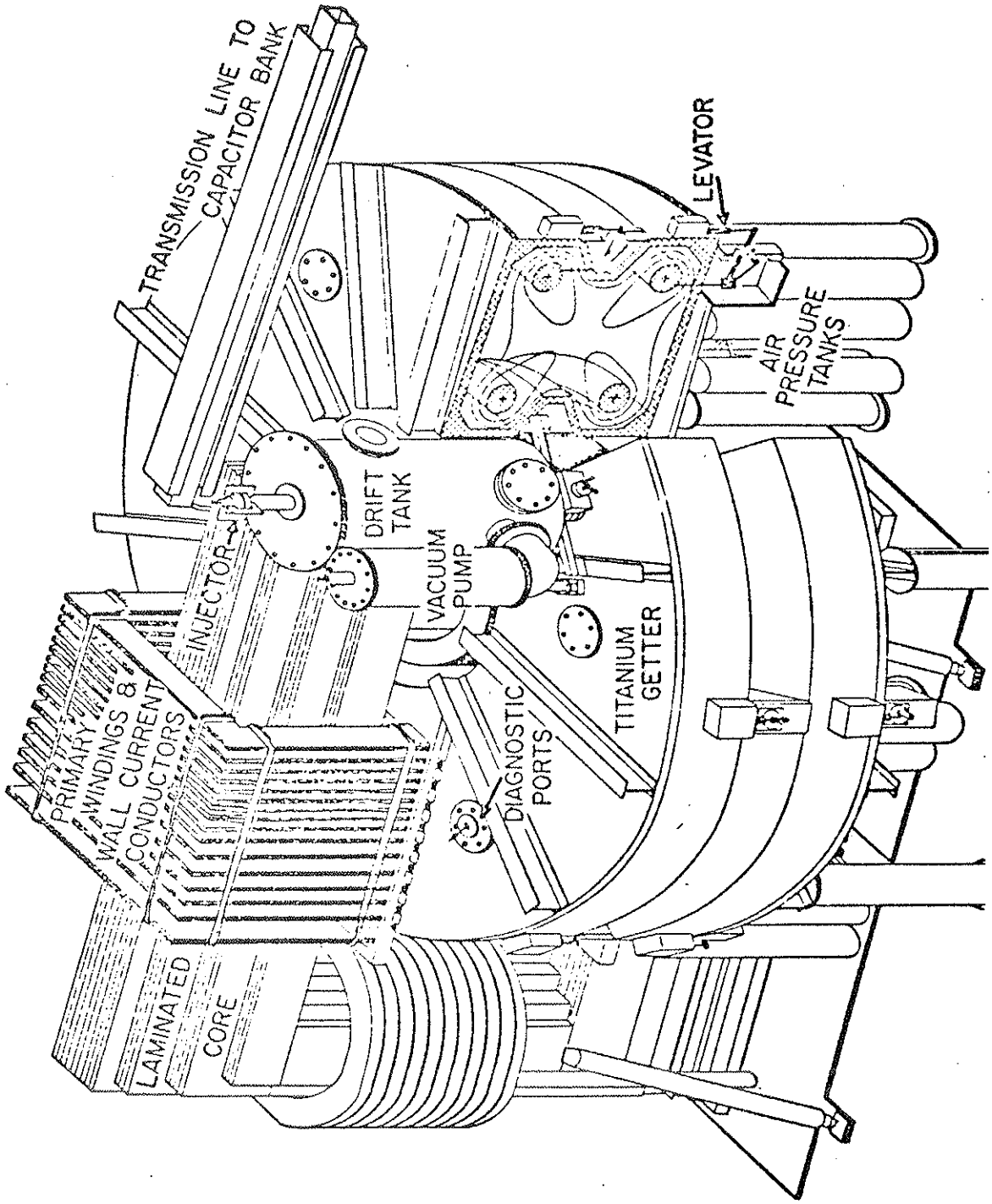
TRANSMISSION LINE TO CAPACITOR BANK
LEVATOR
AIR PRESSURE TANKS
DRIFT TANK
VACUUM PUMP
INJECTOR
TITANIUM GETTER
DIAGNOSTIC PORTS
PRIMARY WINDINGS & WALL CURRENT CONDUCTORS
LAMINATED CORE

few millimeters. It requires 20 msec to move the supports approximately 10 cm below the rings (this is outside the confinement region), and 20 msec to reinsert them. The total time they are held out, then, is also 20 msec. During the support free period, the rings receive a gravitational impulse which the supports must absorb after reconnection. The ring-support system then undergoes a series of damped oscillations between the final resting position and a point very near the wall. This process is called levitation because at the largest possible magnetic fields, the wall currents help support the rings in position against the gravitational field and the final cushioning oscillations are small. Levitation may be programmed to occur at any time in the field pulse or not at all and in the levitated experiments reported in the later chapters, all supports are fully removed at the time plasma is injected. Table 1 summarizes the major electrical and mechanical features of the device. More complete descriptions are available elsewhere.[1,2,3]

(ii) The Magnetic Field

The machine was designed to have the capacitor bank discharge into the transformer to produce a half sine magnetic field pulse 43 msec long. It then was modified to allow the transmission line to be "crowbarred" (CBR) shortly after peak field, that is, shorted at the capacitor bank. The resulting magnetic field decay rate varies according to position but $B/\dot{B}$ is everywhere longer than 70 msec.[4] It is well known[5,6] that sometime after peak field in the half sine case the Poynting vector at the surface of the rings reverses direction and flux

TABLE I 1

OPERATING PARAMETERS OF THE LEVITATED OCTUPOLE

Capacitance	0.048 F
Maximum Voltage on Capacitors	5 kV
Energy of Pulse	0.6×10^6 J
Maximum Core Flux	0.72 Wb
Inductance L: $L = N^2 L_o$, $N = 90$	$L_o = 0.6$ μH (calculated)
Volume of Vacuum Region	8.6 m^3
Volume inside ψ-critical at 20 msec	7.7 m^3
Ring Minor Radius	8.9 cm
Inner Ring Major Radius	0.99 m
Outer Ring Major Radius	1.79 m
Wall Thickness	5 cm
Half Sine Period (Poloidal Field Only)	43 msec

VALUES AT MAXIMUM CORE FLUX

	Wall	Inner Ring	Outer Ring
Current*	1.4×10^6 A	0.5×10^6 A	0.25×10^6 A
B max (at surface)*	6. kG	12. kG	5.5 kG
B min (at surface)*	1. kG	5.3 kG	3.4 kG

* Approximate values

begins to reemerge from the surface. This occurs between 31 and 32 msec in the field pulse. This effect has a major influence on the bulk motion of the plasma as will be shown in chapter III. Plasma profiles of density and potential for the sine field prior to about 30 msec are similar to those seen for the CBR case. The plasma evolution in the sine field becomes dominated after 32 msec by the motion of the magnetic field.

Figures 2 and 3 show the magnetic field lines in the octupole and the lines of constant magnetic field strength at 25 msec, shortly after the CBR. These diagrams are cross sections of the torus and the field lines close in the plane of the cross section. When rotated about the toroidal axis, the closed field lines generate closed toroidal flux shells which are symmetric about the central axis. In some regions of the torus, all flux shells enclose a single ring, in others, they all enclose two and in yet others all four rings. The magnetic lines which generate the boundaries between these regions are called the separatrices and are the dotted lines of Figure 2. An interesting and important observation is that each separatrix passes through the zero magnetic field strength region. These field nulls act as non-adiabatic scattering centers for any charged particle whose center of gyration about a magnetic field line is within its gyro radius of a separatrix. When the gyration center moves along the field line and enters the field null region, it loses all information about its previous magnetic moment and can scatter into any of the magnetic flux regions of the machine. The final destination depends only on the phase of its orbit about the magnetic field as it enters the field null region. This

Figure 1 2

Cross section of the octupole showing the magnetic field lines at 25 msec into the field pulse. The field lines are numbered with the value of ψ assuming a peak core flux of 10 units.

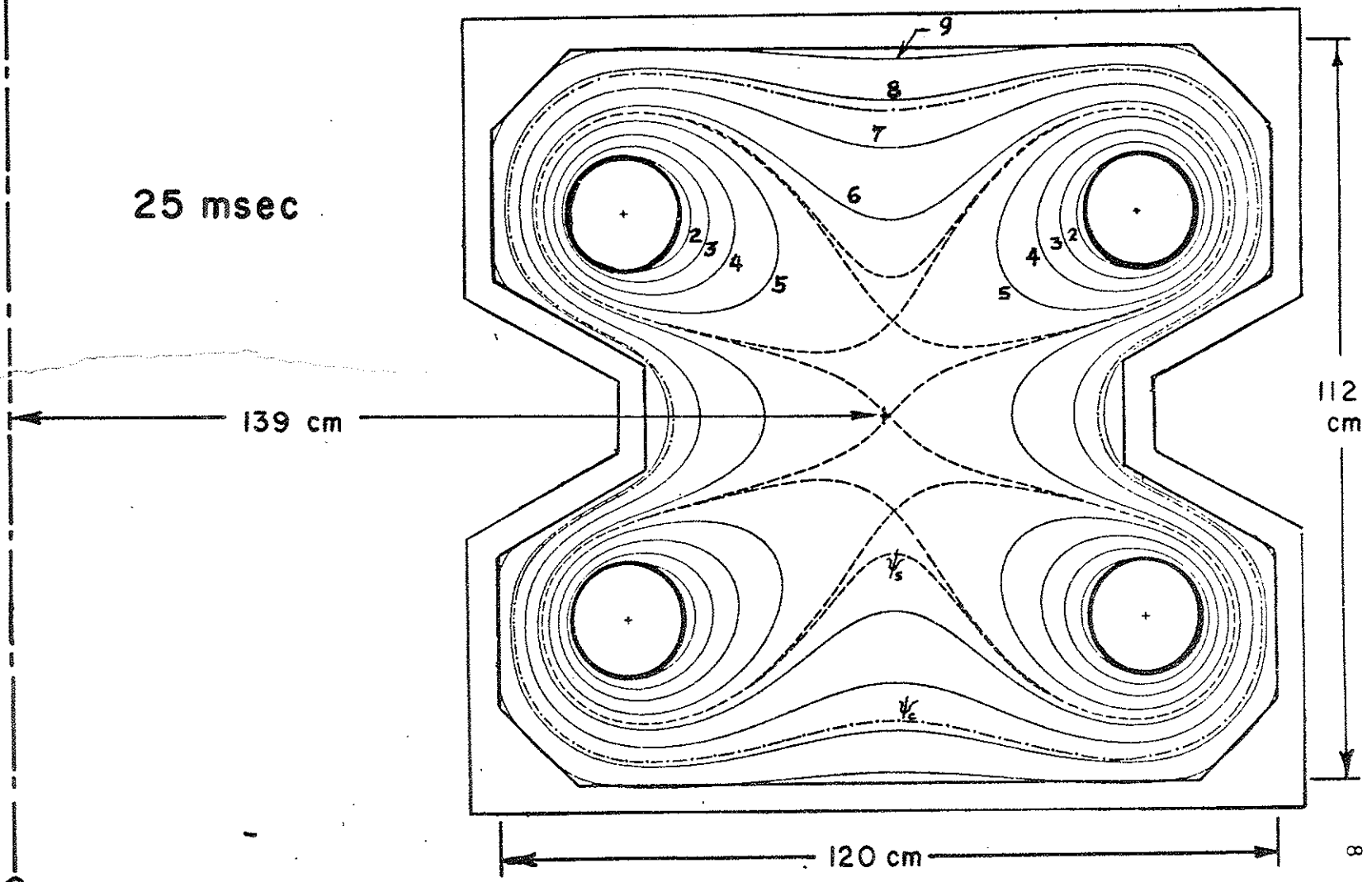
25 msec
139 cm
112 cm
120 cm
9
8
7
6
5
4
3
2
ψ_s
ψ_c

Figure I 3

Cross section of the octupole showing $|B|$ at 25 msec.

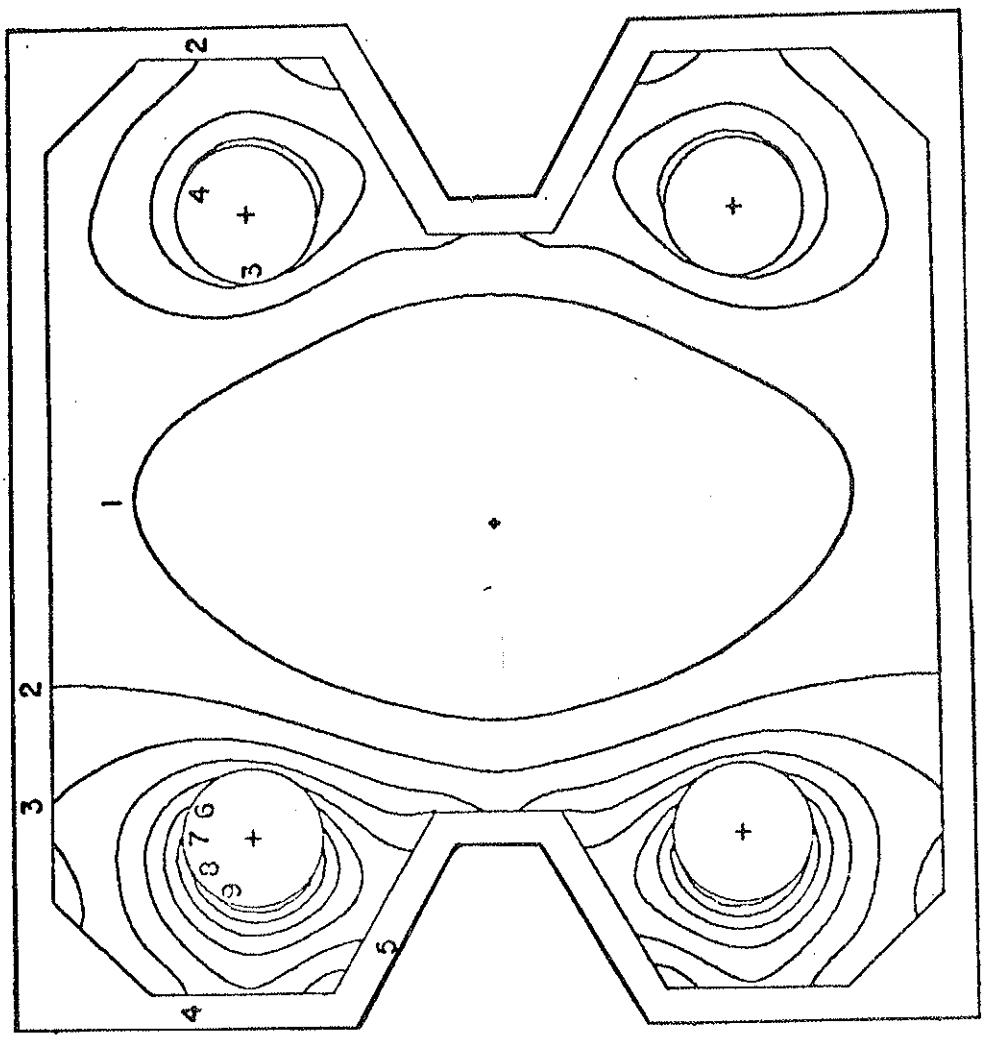

|B| kG
25 msec

process has been discussed by others[7,8] and is partially responsible for maintaining continuity of the plasma parameters (density and temperature) across the various regions.

(iii) Flux Coordinates

It is convenient for the purposes of the following discussion and for the work of the later chapters to employ flux coordinates which are non-linear in the usual Cartesian "x,y,z" spatial coordinates but which provide a geometry-independent description of the processes occuring in a magnetic device. Flux coordinates are fully described elsewhere.[9] For the purpose of orientation, envision two axes for a torus: a linear "toroidal" axis which is the symmetry line of rotation used in Figure 2 to produce the torus from a cross section, and a circular "mid circle" axis which runs through the center of the "donut" and encircles the toroidal axis. In Figure 2, the mid circle would be the locus of the central field null under rotation about the toroidal axis. The "mid cylinder" is the figure generated by moving the mid circle parallel to the toroidal axis. The toroidal position is provided by the azimuthal angle ζ measured about the toroidal axis along the mid circle. The poloidal position (the short way around the torus, in the plane of the cross section of Figure 2) is specified by the poloidal magnetic scalar potential χ which is measured along a field line in the direction of $\underline{B}$. The third coordinate is the total magnetic flux ψ between the toroidal axis and point in space being identified (including the core flux). It may be shown[9] that ψ is a constant along a field line and is the coordinate used to label the flux shells described above. It serves as a

radial coordinate for the set. The coordinate directions are oriented by the fundamental relationship $\underline{B} = \nabla\chi = \nabla\psi \times \nabla\zeta$. ψ is zero inside the rings (if super conducting) and increases for flux shells successively further from any ring. Since $\hat{\chi}$ is parallel to $\underline{B}$, $\hat{\zeta}$ must be opposite the direction of the ring current.

The field lines of Figure 2 are labeled with the calculated value of ψ. The convention used for the calculation is the assumption that the core contains 10 units of flux at peak field. The units of ψ are named for Dory, who originated the convention. The conversion from the tabulated value ψ_t to the actual value is $\psi = A\psi_t$ where A is .1 times the actual core flux ϕ_c. ϕ_c is easily calculated to be $(LC)^{1/2}\ V_c/N$ where N is the number of turns on the transformer. L, C, and N are obtained from Table 1 and A is $1.52 \times 10^{-2}\ V_c$ Wb/d where V_c is the initial capacitor bank voltage in kV. Drake[10] has measured ϕ_c and gives the experimental A to be $(1.45 \pm .04) \times 10^{-2}\ V_c$. Figure 4 plots $\psi_t(x)$ v.s. position in centimeters across the outer bridge which is the region between an outer ring and the outer wall. ψ_t is shown for various times in the half sine pulse. The $\psi_t(x)$ for the CBR field is assumed to be given by the 25 msec curve. At 25 msec, the separatrices are near 5 cm, the flux lines ψ_g that just graze the walls are near 10 cm, and the flux line ψ_c which separates the region of stably confined plasma from the outer region near the wall of unstable plasma is near 9 cm. The arrow heads indicate the direction these surfaces move in time.

There will be occasions in later chapters when a representative value for the magnetic field is desired for a given flux surface.

Figure I 4

The flux function $\psi_{(t)}$ v.s. position in the outer bridge region, between the ring and the wall. $\psi_{(t)}$ is calculated assuming that the peak magnetic flux in the core is 10 units.

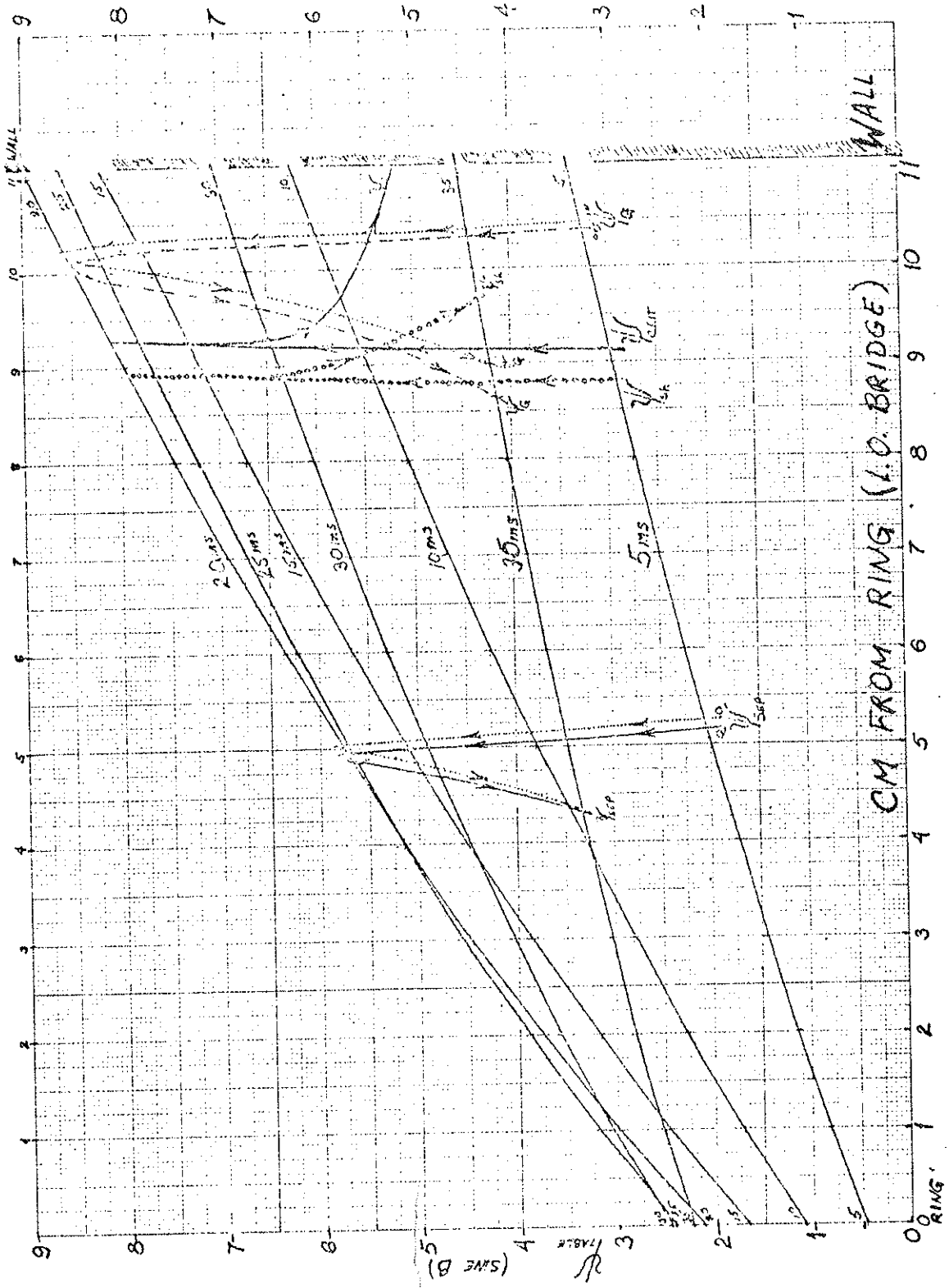
WALL
CM FROM RING (L.O. BRIDGE)
RING
(SIDE B)
TABLE
20 m/s
25 m/s
15 m/s
30 m/s
10 m/s
35 m/s
5 m/s

Figure 5 plots the actual magnitude of the magnetic field in kG v.s. ψ at 25 msec for an initial capacitor bank voltage of 2.5 kV. Several average values are given, the maximum and minimum values along the line, as well as the values for the outer bridge region (between an outer ring and the wall) and the mid cylinder. The average of B around a field line is $\langle B \rangle_l = \oint \underline{B} \cdot d\underline{l} / \oint dl$ where the integration is along the field line and $d\underline{l} = \hat{\chi} d\chi / B$. The average of B along a tube of constant flux is $\langle B \rangle_{V'}$. It has been shown elsewhere[11] that the flux tube average of a quantity A is $\langle A \rangle_{V'} = (\oint A\ dl/B)/(\oint dl/B)$ so $\langle B \rangle_{V'} = \oint dl / \oint dl/B$. The values for the integrals are from computed tabulations.[12]

B: Plasma

There are a number of different mechanisms available for generating plasma in the octupole but in general they fall into one of two classes: (a) hot ion, relatively low density plasma with low neutral pressure, and (b) cold ion, higher density plasma with high neutral background pressure. The principle source for the hot plasma is the small coaxial gun of the type described by Marshal[13] and others,[14,15] mounted on the end of the drift tank outside the toroidal chamber (Figure 1). The gun fires its plasma into the torus through a 10 cm aperture and its neutrals are initially deposited in the drift tank. A nude ion gauge in the torus indicated[16] that the neutral gas enters with about a 10 msec rise time. The ambient background pressure in the torus is typically 1 to 2×10^{-7} Torr, just prior to injection of the hydrogen plasma and the initial electron-neutral collision time is

Figure I 5

Representative values of the magnetic field B, in kG, v.s. the ψ of Figure I 4 assuming that the main capacitor bank was charged to 2.5 kV. $\langle B \rangle_V$, is the average of B over the flux tube, $\langle B \rangle_\ell$ is the average around the field line.

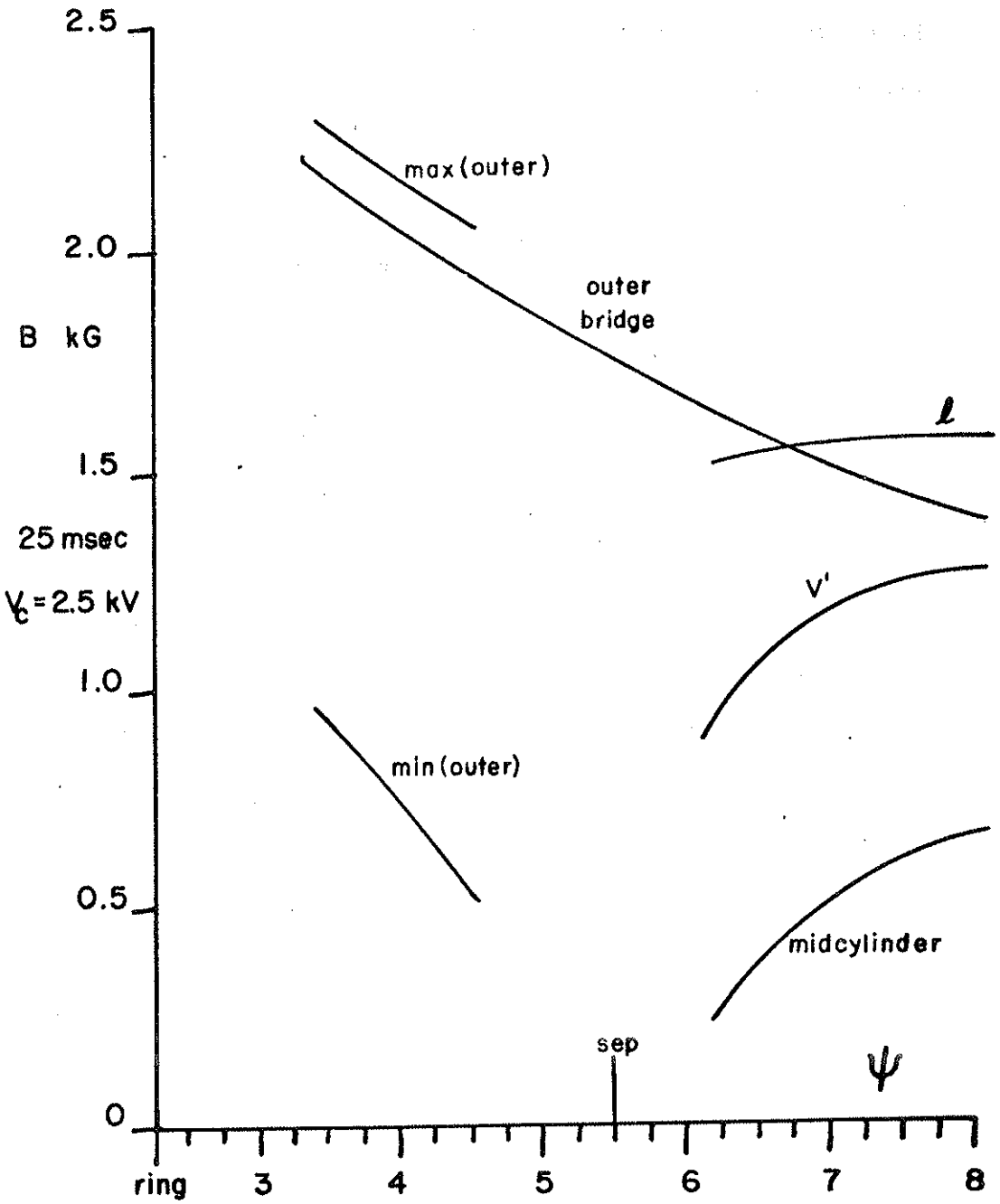
2.5
2.0
B kG
1.5
25 msec
V_c = 2.5 kV
1.0
0.5
0
max (outer)
outer
bridge
ℓ
V'
min (outer)
midcylinder
sep
ψ
ring
3
4
5
6
7
8

about 2 msec. A helium cooled cryo panel was installed for the majority of the work reported here so the principal initial background constituent is H_2, as seen by the residual gas analyser installed on the torus. The ion temperature is about 30 eV one millisecond after injection and the electron temperature is 8 eV. Table 2 presents the important plasma parameters for this plasma. The details of their measurement are presented in later chapters.

The cold, dense plasma is produced by either one of the microwave sources or by a somewhat larger gun which discharges directly into the torus.[17] Both plasmas are associated with neutral pressures of at least the upper 10^{-6} Torr region with electron-neutral collision times of less than 100 μsec. The initially hot ions from the large gun are known to drop in temperature below measurability within the first few milliseconds. The principal advantage of these plasmas over the hot plasma from the small gun is the high particle density, 10^{10} to 10^{12} cm^{-3}, and the high degree of reproducibility. Microwave plasma typically exhibits shot-to-shot variation in its parameters of less than 5% while the drift tank gun user must accept 10 to 20% variation. The high density readily allows probe measurements of most parameters such as potential and density, while the low density plasma measurements have problems because of large debye length and high sheath impedance (see Chapter II). The principal disadvantages are the ion temperature and high collisionality. Thermonuclear plasmas will be nearly collisionless due to their extremely high temperature. In addition, finite ion gyro radius effects should be expected in these plasmas. Neither of these operating regimes are available to cold, high density plasma

TABLE I-2

WISCONSIN LEVITATED TOROIDAL OCTUPOLE

OPERATING PARAMETERS (RINGS LEVITATED AT INJECTION)

	PEAK VALUE IN MACHINE ONE mSEC AFTER INJECTION	E-FOLDING TIME OF PEAK VALUE
$\|B\|$	5 kG (POLOIDAL ONLY)	-70 msec
NEUTRAL PRESSURE	1×10^{-7} TORR PRINCIPALLY H_2	+10 msec
HYDROGEN PLASMA DENSITY	8×10^{9} cm^{-3}	-18 msec
ELECTRON TEMPERATURE	8 eV (SPATIALLY UNIFORM)	-30 msec
ION TEMPERATURE	30 eV (SPATIALLY UNIFORM)	-11 msec

Table I-2

and it is for this reason that hot ion plasma was chosen for the investigations presented in the later chapters.

Effects of collisionality may be investigated in a controlled manner by puffing neutral gas into the torus just prior to injection. The reproducibility of the gun is another problem. Figure 6 presents three series of oscilloscope records of plasma shots taken to show the gun behaving in different manners. These records were taken weeks apart. The traces are of the plasma current drawn to a single tipped probe biased at -45 V to repel electrons and located on the separatrix in the lower outer bridge region. It is shown in chapter II that such current is proportional to ion density times the square root of the temperature. All three sets are triggered at the beginning of the field pulse and sweep at 5 msec per division across the photographs. The machine operating parameters are the same in all three cases: B_p only, supported rings, V_c of 2.5 kV, and the torus pressure of about 1×10^{-7} Torr. Figure 6(a) shows the optimal behavior of the gun. The records of ten shots are seen to overlay one another within a 5% deviation. In addition, one levitated trace is shown and demonstrates the fact that levitation causes a factor of 2 increase in the drawn current. An acceptable plasma variation is shown in (b) which is the overlay of 5 shots. This is a typical variation in the gun parameters and appears to be due to variations in the plasma density. Figure 6(c) shows an unacceptable case where the behavior of the gun was pathologically bad. Such behavior is presumably caused by wide independent variation of density and temperature. The gun must be removed from the system at this time and cleaned. Visual inspection of the gun elec-

Figure I 6

Ion saturation current drawn by the same probe biased to -45 V at ψ_s, 225° lower outer bridge region. Triggered on field pulse, horizontal sweep at 5 msec/division. Gun injection of hydrogen at 25 msec into CBR field. V_c = 2.5 kV, $P_T \simeq 1 \times 10^{-7}$ Torr.

(A) 10 supported ring traces, 1 levitated trace, 100 μA/D. This is optimal plasma from gun with newly polished electrodes.

(B) 5 acceptable traces, 50 μA/div, rings supported.

(C) 7 unacceptable shots, 50 μA/div, rings supported. After removal of gun, electrodes showed discoloration and severe arcking patterns.

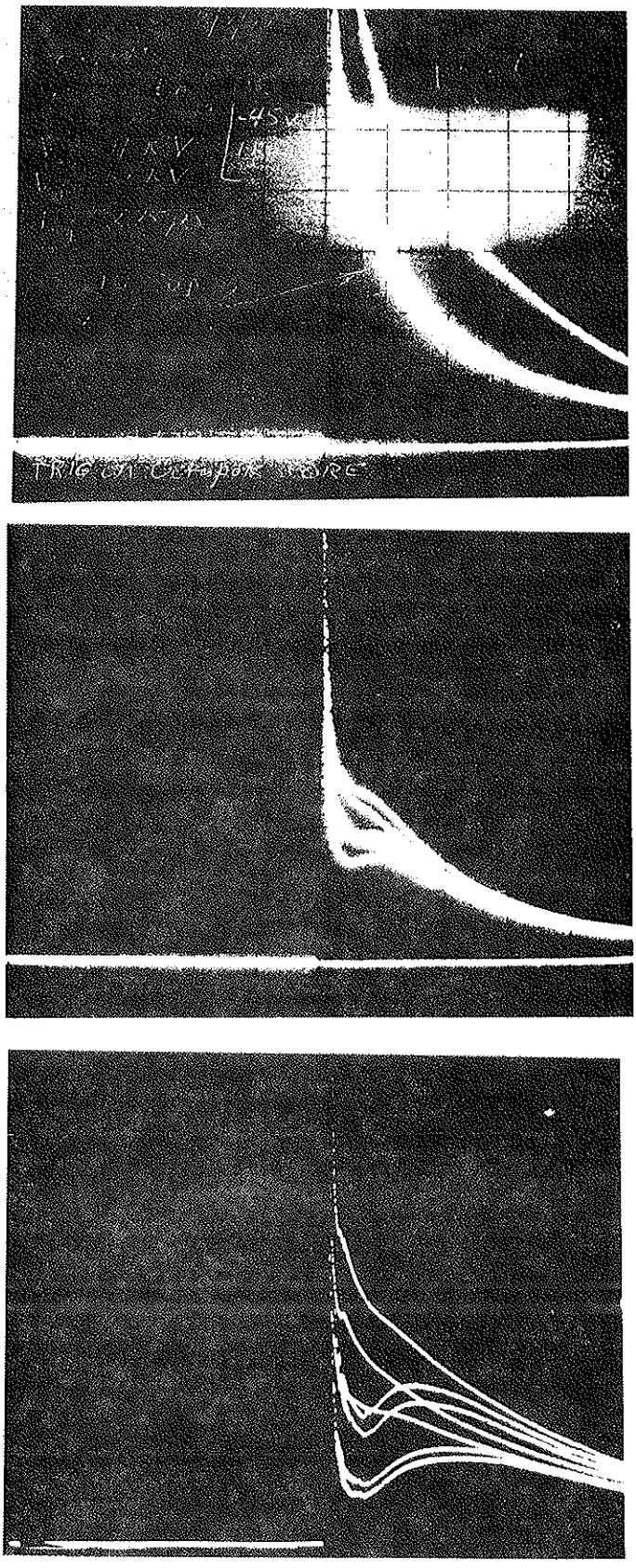

A

B

C

trodes shows surface scarring due to improper arcking of the plasma in the gun. Inspection of the gun surfaces after operation in mode (a) shows no such surface problems. The operation modes of (b) and (c) may generally be restored to that of (a) by careful polishing of the electrodes before reinstallation. Mode (c) has also been caused by external arcking of the plasma between the gun's outer electrode and the conductive drift tank wall. The distribution of plasma inside the octupole for this case is documented in Chapter III. An extender was provided for the outer electrode which moved the muzzle of the gun further from the drift tank lid and appears to solve the external arcking problem. For reproducibly smooth behavior of the gun, it was found necessary to remove and repolish the electrodes every several weeks, after about a thousand shots. This record compares well with what the investigators who develop gun design call reproducible.[18] Such guns are specially assembled, tested for 50 to 200 shots, then disassembled and modified (and cleaned!). Plasma from such guns are reputed "always" to look like Figure 6(a).

Figure 7 is included here for later reference. It plots the gyro radius ρ of a 20 eV proton as a function of the tabulated ψ_t for the octupole field when V_c is 2.5 kV. Shown are the flux tube and line average of ρ which are equivalent to the averages of B^{-1} and the specific values for ρ in the bridge and along the mid cylinder.

Figure I 7

Representative values of the ion gyro radius $\rho_i(\psi)$, in mm, v.s. ψ for T_i = 20 eV hydrogen, V_c = 2.5 kV.

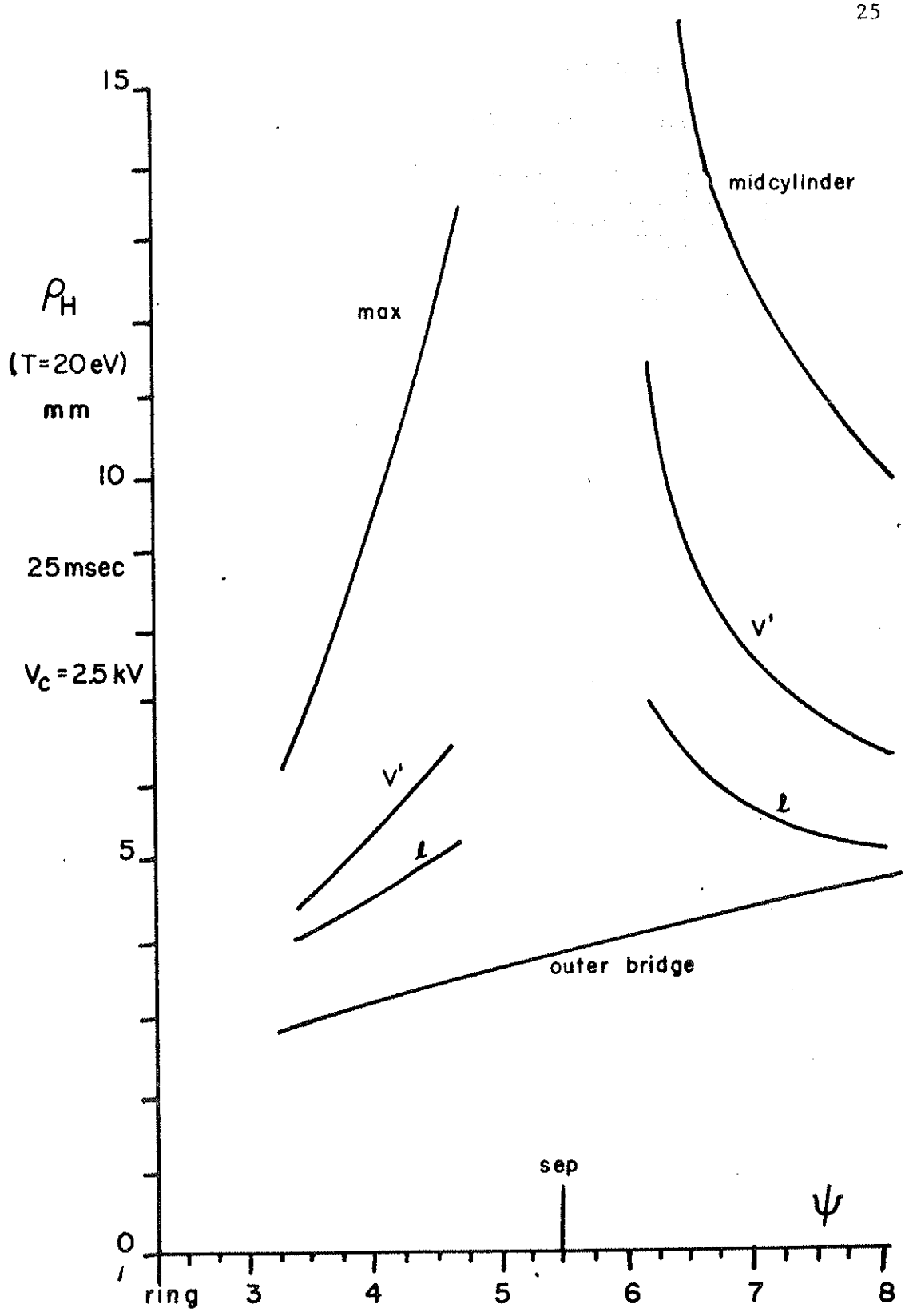
15
10
5
0
ρ_H
(T=20eV)
mm
25msec
V_c = 2.5 kV
midcylinder
max
V'
V'
ℓ
ℓ
outer bridge
sep
ψ
ring
3
4
5
6
7
8

REFERENCES FOR CHAPTER I

1. J. Steben. J. Appl. Phys. 43, 1211 (1972)

2. H. K. Forsen, D. W. Kerst, R. A. Breun, A. J. Cavalo, J. R. Drake, J. C. Sprott. Proceedings of the Fourth European Conference on Controlled Fusion and Plasma Physics (Comitato Nazionale Energia Nucleare, Rome, 1970), p. 24

3. I. N. Sviatoslavsky, N. C. Lien. Hydraulics and Pneumatics (Sept. 1971) p. 86 and PLP-275 (1969)

4. G. A. Navratil. University of Wisconsin Plasma Physics PLP-629

5. K. Evans. University of Wisconsin Plasma Physics PLP-464

6. J. Schmidt. University of Wisconsin Plasma Physics PLP-181

7. M. G. Rusbridge. Plasma Physics 13, 977 (1971)

8. B. Lehnert. Plasma Physics 17, 501 (1975)

9. C. J. Armentrout. University of Wisconsin Plasma Physics PLP-667

10. J. R. Drake. University of Wisconsin Plasma Physics PLP-512

11. C. J. Armentrout. University of Wisconsin Plasma Physics PLP-470

12. A. Butcher Ehrhardt. University of Wisconsin Plasma Physics PLP-703

13. J. Marshal, Phys. Fluids 3, 134 (1960)

14. C. E. Bush. Ph.D. Thesis. University of Wisconsin (1972)

15. C. E. Bush, H. K. Forsen, H. de la Fuente, R. Harder, G. Kuswa. University of Wisconsin Plasma Physics PLP-146

16. D. A. Brouchous. University of Wisconsin Plasma Physics PLP-648

17. G. A. Navratil. Ph.D. Thesis. University of Wisconsin (1976)

18. D. Y. Cheng. Bul. Am. Phys. Soc. 21, 1175 (1976)

CHAPTER II: DATA ACQUISITION AND ANALYSIS TECHNIQUES

A: Probes

(i) Physical Construction

The basic tools for acquiring the data presented in later chapters are high and low impedance probes. These have been discussed in detail many places.[1,2] Figure 1 shows the diagrams of the three probe constructions used in this work. The tips of all three probes are smaller than an ion gyro diameter (>6 mm) so the ion flux to the tips may be assumed to be isotropic. The high Z probe consists of a tungsten cylindrical tip sealed with epoxy in a glass tube. A 20 MΩ resistance was placed just behind the tip and shielded by a copper foil electrically connected to the tip. Grounded shield coaxial cable was connected to the resistor and led to a "probe box" which provided a frequency-compensated voltage divider and an amplifier. Full description of the circuits used is found elsewhere.[2] This probe was used to acquire the early injection data of Chapter V.

The type 1 low Z probe consists of a cylindrical copper tip epoxyed to a hypodermic needle which is in a teflon sleeve. The needle is electrically connected to ground through the stainless steel main body of the probe. The tip is connected via a wire to grounded shield coaxial cable which leads to the outside world. For frequencies below 500 kHz, it was found that the same response could be obtained for this probe attached to a Tektronix 10×, 10 MΩ attenuating probe as for the 20 MΩ high Z probe with the balance box and amplifier just described. Since this probe has the additional advantage of presenting a smaller

Figure II 1

Diagram of three basic probe types used in the experiments.

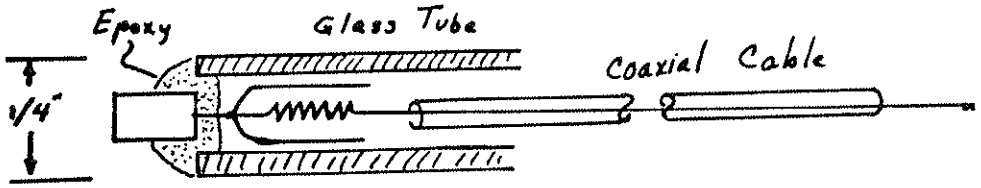

HIGH Z

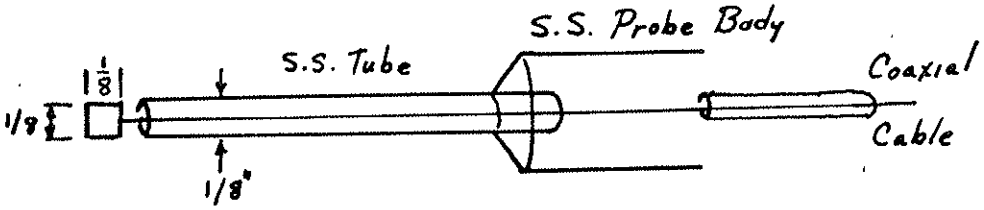

LOW Z 1

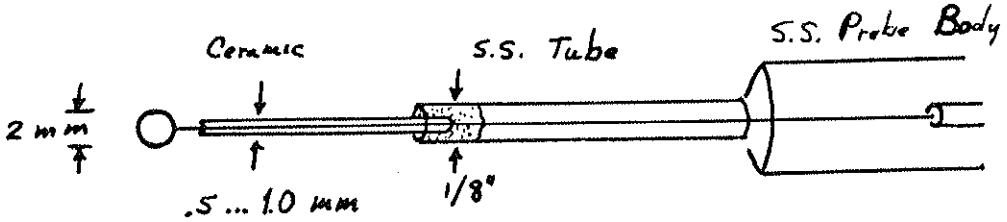

LOW Z 2

profile to the plasma, it and the type 2 probe are used in the majority of the experiments.

The type 2 probe is similar but the tip is a small sphere on the end of a thin ceramic stalk. Both platinum and gold were used for the tips but platinum has proven to be most useful because of its high melting temperature and ease of handling. In addition, pure platinum may be purchased while gold is always alloyed, usually with copper. The gold-tipped probe has proven to suffer from problems with surface contamination (see below). The ceramic stalk leads to the hypodermic needle of the type 1 probe.

It is important to bring the coaxial shielding as close to the tip as possible to avoid capacitative coupling to plasma fluctuations which are distant from the tip. R. Richards has reported[3] that for the same D.C. plasma, a major difference was observed between the measured potential signals from two probes which differed by the presence of coaxial shielding along the stalk of one. The shielded stalk allowed him to obtain a consistent phase relationship between potential and density fluctuations, which was not obtainable from the unshielded probe.

For all probes of type 2, the ceramic stalk is at least 1 cm long, however. Large obstacles generate turbulence which affects the measurements of a second probe. It is for this reason that the high Z probe was abandoned and the low profile type 2 probe is preferred for all fluctuation measurements.

(ii) Simple Probe Theory

A number of problems arose when these probes were used. As indicated below, they are the result of the expansion of the plasma sheath as a function of probe tip bias, and of surface contamination of the probe tip itself. These problems may be understood using "simple probe theory" which ignores the presence of a magnetic field and the expansion of the sheath. Full details may be found elsewhere.[4]

Probe theory treats the ion or electron collection by an object embedded in the plasma. If the object is at any potential other than the plasma's potential, V_p, a space charge layer called the sheath forms which shields the plasma from the object's potential V. "Simple" probe theory assumes that the ions and electrons have a Maxwellian velocity distribution and that the sheath's thickness is independent of $\Delta V = V - V_p$. This discussion will use the thin sheath approximation where the sheath area is the same as the probe tip area.

Figure 2(a) shows the equivalent circuit for such a probe with impedance R_m to the laboratory ground. For $\Delta V < 0$, all ions incident on the sheath are collected and accelerated[4] to the ion sound speed $c_i = (eT'/2\pi m_i)^{1/2}$. Here, m_i = ion mass, $T' = T_i$ for $T_i > T_e$ or is T_e otherwise. All temperatures are expressed in volts. The sheath retards the electrons so $R_s \equiv R_e$ is the electron current impedance which grows as $\exp(|\Delta V|/T_e)$. For a tip which is deeply enough biased, $|\Delta V| \simeq 3 \ldots 5 \times T_e$, the current drawn has a saturated value given by the isotropic ion flux

$$I_{io} = \frac{1}{4} n_i A \left(\frac{T'}{2\pi m_i} \right)^{1/2} . \qquad \text{[II-A-1]}$$

Figure II 2

(A) Equivalent circuit for a single tipped probe.

(B) Characteristic plot of the current I(v) drawn to a probe tip v.s. the tip's bias voltage.

(A)

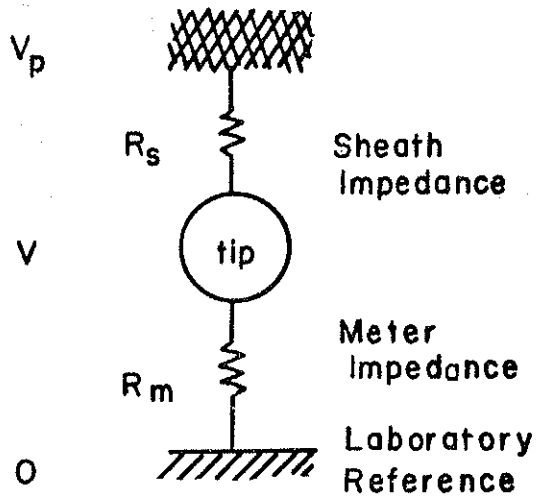
V_p
R_s
Sheath Impedance
V
tip
Meter Impedance
R_m
Laboratory Reference
0

(B)

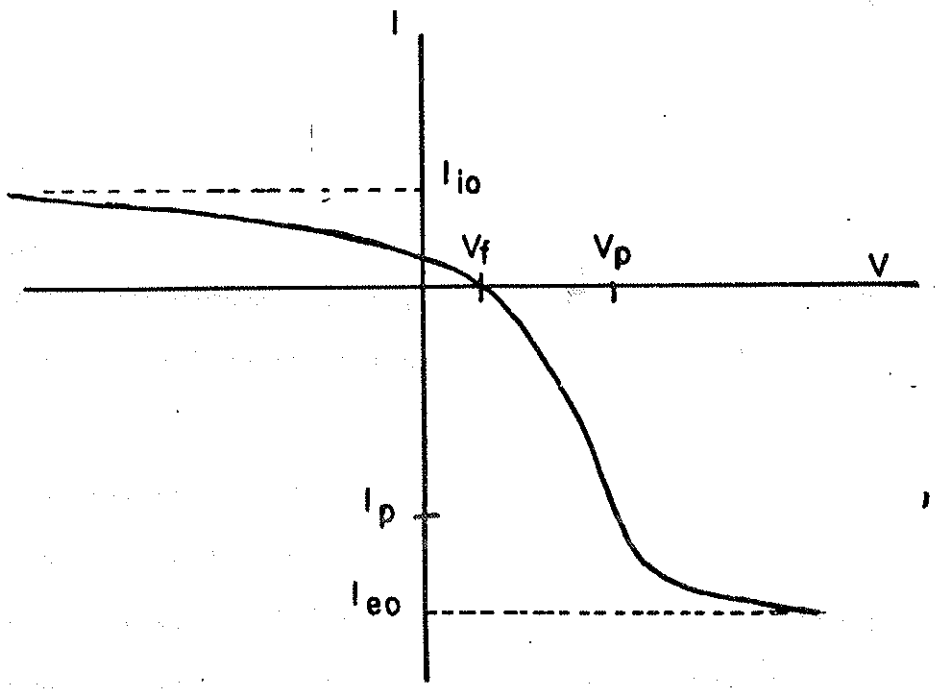
I
I_{io}
V_f
V_p
V
I_p
I_{eo}

For $\Delta V > 0$, the situation is reversed and $R_s = R_i$ is the ion current impedance which grows as $\exp(\Delta V/T_i)$. Figure 2(b) shows the characteristic graph of probe bias versus current drawn. When no net current is drawn by the probe, the tip bias is called the floating potential, V_f. An isolated object will charge to V_f and draw no further net current. It is easy to use $I_{io} = I_{eo} \exp(V_f - V_p)/T_e$ to show that (v_e = the electron thermal speed)

$$V_f = V_p - T_e \ln(v_e/c_i) \qquad \text{[II-A-2]}$$

$$R_s = \left(\frac{T_e}{neA}\right)\left(\frac{2\pi m_i}{eT'}\right)^{1/2}. \qquad \text{[II-A-3]}$$

The relation for the sheath impedance, R_s, evaluated at $V = V_f$, is given by Sprott.[5]

(iii) Effects of Sheath Expansion

More realistic probe theories[6,7,8] show that the expansion of the sheath modifies the saturated (constant) value of I_{io} in [1] into a nearly linear function of $(V_f - V)$. Rudmin has verified[9] that the predicted shape of the characteristic graph for a probe is very nearly that which is actually observed.

One interesting feature is that the floating potential can vary by as much as 3 or 4 T_e across flux space at any instant. Such plasma profiles are presented in Chapter III. This will cause misinterpretations if simple probe theory is used to construct density profiles from the current drawn by a probe biased to repel electrons. Figure 3 illustrates this point. Consider the exaggerated case of a constant

Figure II 3

Characteristic plots for a probe with a fixed bias V_b at two positions in a plasma with a potential gradient but no density gradient. The operating points of the probe are marked by an x.

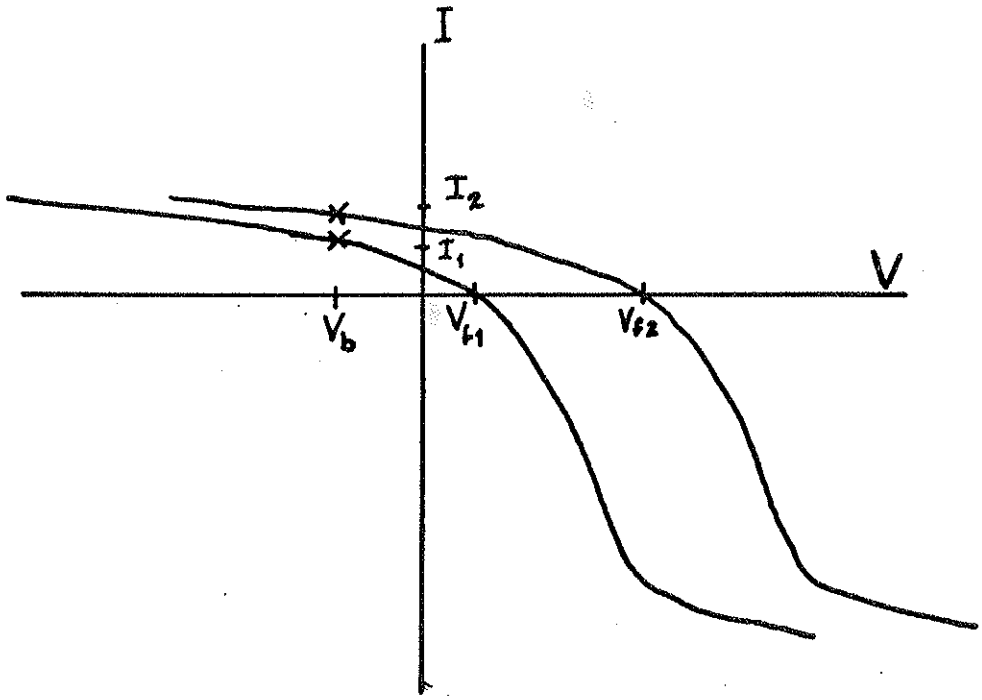
I
I_2
I_1
V
V_b
V_{t1}
V_{fz}

density profile (i.e., one with no density gradients), but with a large potential gradient. Two identically shaped characteristic probe curves are drawn for the two different positions in the plasma. A fixed probe bias is assumed and the two currents drawn by the probe are marked by the x's. An observer who uses simple probe theory to obtain a density profile as is commonly done[10,11] would obtain a density gradient proportional to the potential gradient. One method of circumventing this problem is to bias the probe more deeply into the ion collection branch. A deep bias of $5 \times V_f$ for the octupole would be about -150 V. Before the data from this biased probe could be used, however, one would need to show that the flux tubes were not depleted of ions, especially in the private flux region where the field lines are short.

(iv) Double Probes

A second method, and the one adopted here, would be to use a low impedance double probe[12] as illustrated in Figure 4. Suppose initially $V = 0$. Then both tips 1 and 2 would be at V_f. As V increases, tip 2 moves up the probe characteristic curve drawing ions. Tip 1 rides down the exponential curve collecting electrons until the electron current to 1 equals the ion current to 2. These final points are controlled by T_e, T_i, and n, but are independent of V_f. Figure 4 shows the circuit used in all double probe measurements for the isolated microammeter schematically shown in Figure 5. There is 10^{13} Ω isolation between the diode ammeter circuit and the optically driven differential amplifier circuit. For the circuit shown, the transconductance $I_{through}/V_{out}$ is an essentially constant value from 5 μA to 10 mA. Figure 6 shows

Figure II 4

(A) Circuit schematic for double probe operation.

(B) Diagram illustrating the principle of operation.

(A)

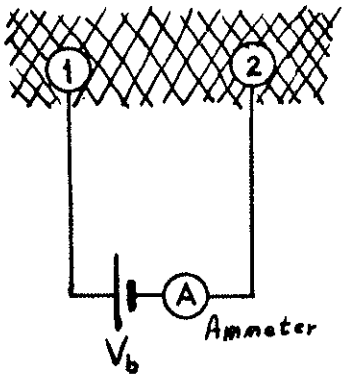

(B)

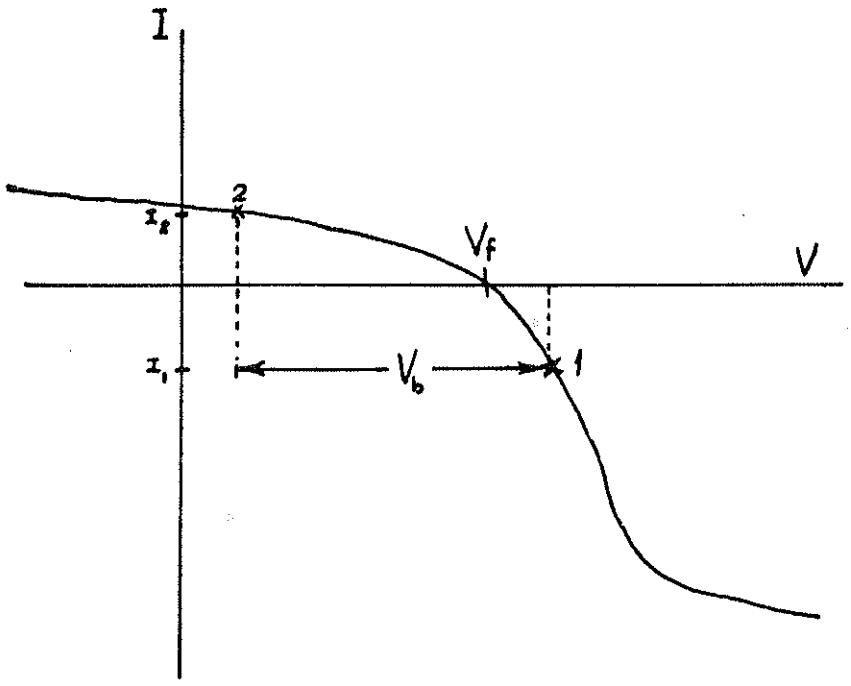

Figure II 5

Circuit diagram of an optically isolated microammeter for the circuit of Figure 4 A.

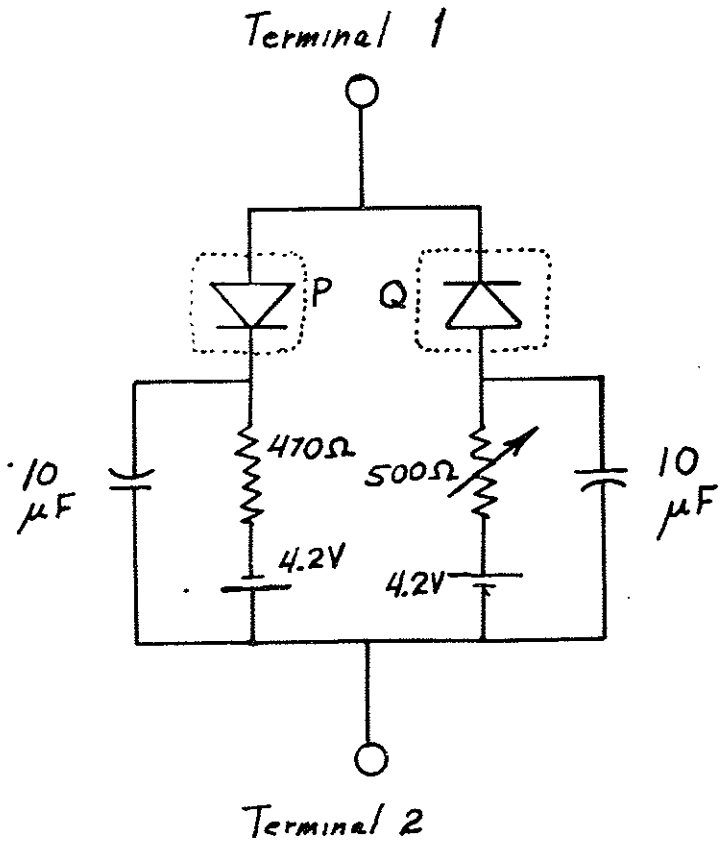

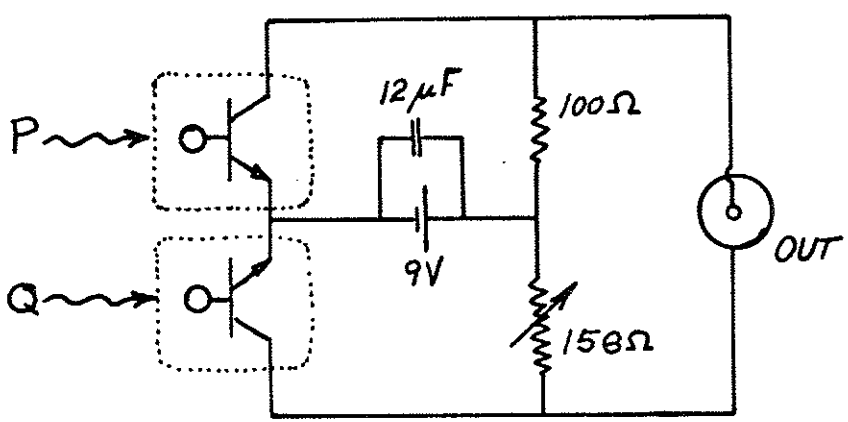

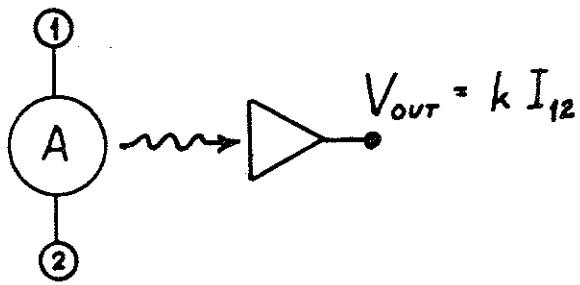

P, Q = MCT-2 Opto-isolator

Figure II 6

(A), (B) Single tipped probe characteristic for a hot ion gun injected plasma 6 and 11 msec after injection (labeled .031 and .036 on graph). Each point is the average of three to five points. Vertical units: 76.3 μA/division. Horizontal units: -45 V to +45 V.

(C), (D) Double probe characteristic for the same shots which were used to generate A. Vertical units: 23.2 μA/division. Horizontal units: -45 V to +45 V.

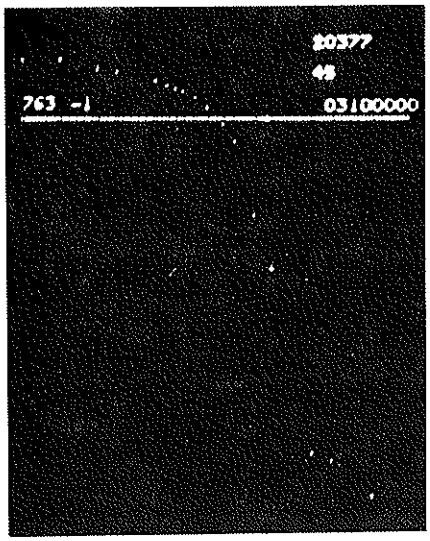
20377
48
763 -1
03100000

A

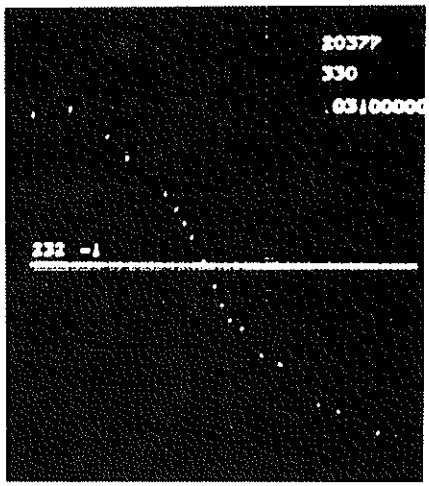
20377
330
232 -1

C

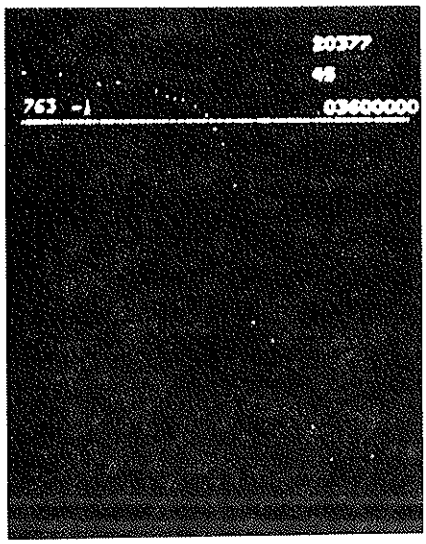
20377
48
763 -1
03600000

B

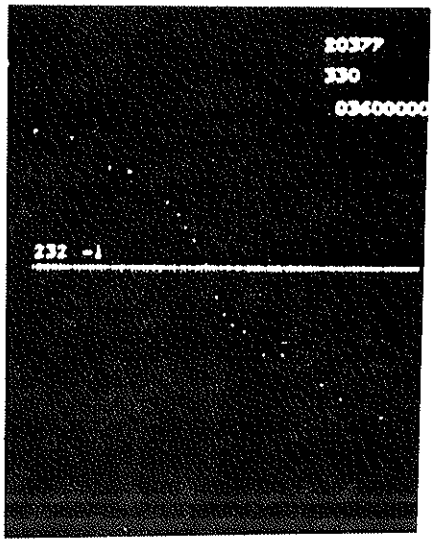
20377
330
232 -1

D

double and single probe characteristics taken for the same set of pulses taken at ψ_s in the B_p supported octupole. For the density profiles of Chapter III, the floating double probe has a relative bias of 45 V which places the ion collecting tip well into the repelled electron branch of the curve.

(v) Surface Contamination

The existence of contaminates on the surface of a probe tip generates a wide range of problems. Many of the difficulties have been studied previously.[13] Only those aspects of the problem will be discussed here which have a direct bearing on the studies presented in the later chapters. The faulty measurement of both density and floating potential profiles is probably the most obvious error caused by surface contamination.

1. Saturation Current Measurements: It is clear, even from the simple probe theory of [1], that a partial coating of the probe tip by an insulating material such as oxide will reduce the effective collection area A and therefore I_{io}. Figure III-29 presents data taken with three separate gold-tipped probes of type 2. When those data were being acquired, the 45° probe initially measured an I_{io} which was 1/3 the value of the other two. All three probes were removed, cleaned with alcohol, very lightly abraded, and then the spark of a hand-held Tesla coil was lightly played over the surface to break up any surviving large areas of oxide. The probes were reinserted and all readings were within ten to twenty percent of each other. If a double probe is also to yield a reasonable estimate of n, both tips must have nominally

the same collection area. It is essential that the tips be clean.

2. Floating Potential Measurements: V_f may be measured by making the impedance, R_m, in Figure 2(a) much larger than the sheath impedance. Equation [3] shows that R_s can be very large for a low density hot plasma[2] and the criterion that $R_m >> R_s$ may be difficult to meet. If $R_m \simeq R_s$, the laboratory ground will be an electron source or sink (depending on the sign of V_f) for the sheath with an "output" impedance comparable to that of the plasma. The operating point for the tip will drift to the region where fewer (or more) plasma electrons are collected and the measuring instruments will no longer read V_f.

A contamination coating on the tip can only worsen the situation. Figure 7 shows the equivalent circuit for a probe tip with a surface coating, such as an oxide, whose impedance is R_c. The tip voltage measured by the experimenter is $V_1 = [R_m/(R_m + R_c)]V_f$, assuming that $(R_m + R_c) >> R_s$. V_1 may be significantly reduced from V_f if the high resistivity contaminate is very thick. A factor of 2 increase in the magnitude of V_f has been observed after cleaning a badly oxidized (i.e., dark, cloudy surfaced) gold ball tip of a type 2 probe. It is pertinent here to re-emphasize that pure gold is very difficult to obtain because it is usually alloyed with copper which has severe oxidation problems. The best material for a probe tip is platinum, which is easily obtained pure, has a high melting point, and is quite non-reactive.

This contamination problem has important implications both for measurements of floating potential profiles, which are done with a single tip, and for direct measurements of the local electric field E

Figure II 7

Equivalent circuit for a probe tip with a surface contamination layer.

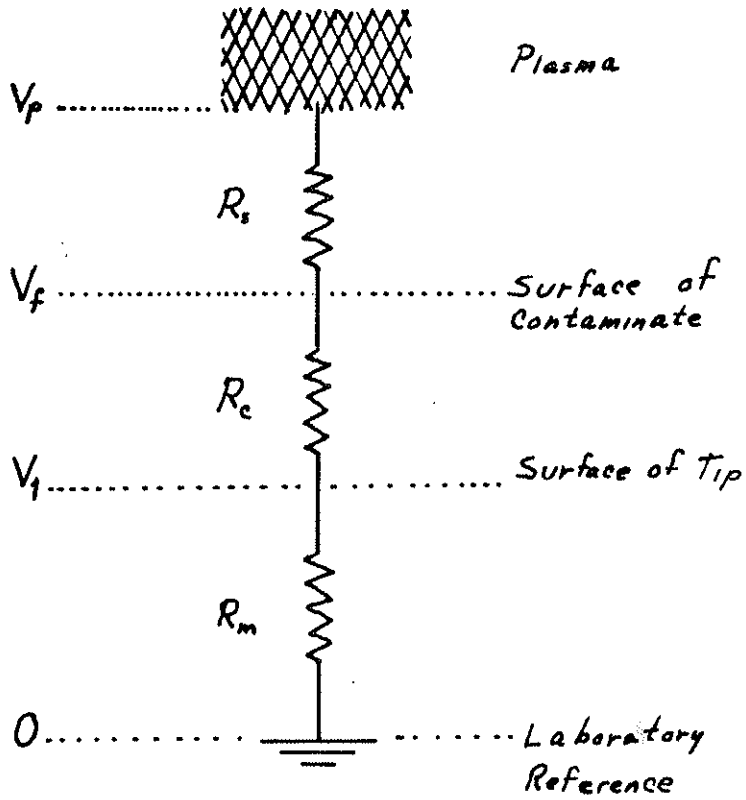
Plasma
V_p
R_s
V_f
Surface of Contaminate
R_c
V_1
Surface of Tip
R_m
0
Laboratory Reference

by subtracting V_f from two neighboring probes. Electric field measurements are especially suspect because R_c will certainly have different values for different tips. In the course of these studies no electric field has ever been measured which unambiguously retained its value when the tips were interchanged. Figure 8 shows the best subtracted measurements from the "self cleaning" platinum tipped expandable double probe described below. Two V_f signals A and B are connected to the (+) and (-) input terminals of a 1A7A differential amplifier. The amplifier--probe set-up had a 100:1 common mode rejection ratio, which is well below any error visible in the photographs. Figure 8(a) shows three shots. The top trace of each shot is A-B and the bottom is A. The tips A and B are aligned along the same field line. Figure 8(b) shows another three shots of the same electrical connections (A-B and A) but the tips have been rotated 180° with respect to the field line. The subtracted amplitudes are not the same in both cases for both orientations nor are the shapes the same, but they do at least reverse in sign. Gold and tungsten tips, cleaned as well as possible prior to insertion, when used in this manner have never been observed to reverse. It could easily be true that with a much higher plasma density, the tips might be plasma cleaned and such a measurement might well be meaningful. It should be stressed that this is the <u>best</u> electric field data taken during these studies. The cleaned surfaces of probes inserted through ports exposed to getter shine undergo continuous coating and $\underline{E}$ measurements must not be considered trustworthy. This is also true of the shot-to-shot reproducibility of a probe in the gettering region which is used to trace out a profile of either I_{io} or V_f.

Figure II 8

Test of V_f subtraction. A and B are oscilloscope traces from the experimental arrangement shown in C. A and B show the data from three successive machine pulses and have two traces for each pulse. Two high Z probes (10 MΩ, 100:1 CMRR) are separated by 1 cm along a field line (ψ = 3.4, lower outer bridge, 330°). The tips were made of platinum and were flame cleaned prior to insertion. The upper trace shows the difference signal between tips 1 and 2, and the lower trace shows the signal to tip 1. In A, the tips were arranged as shown in C, and in B they were rotated 180° (interchanged). The scope was triggered 5 msec after injection, the horizontal scale is 5 msec/division, and the vertical scale is .5 V/division.

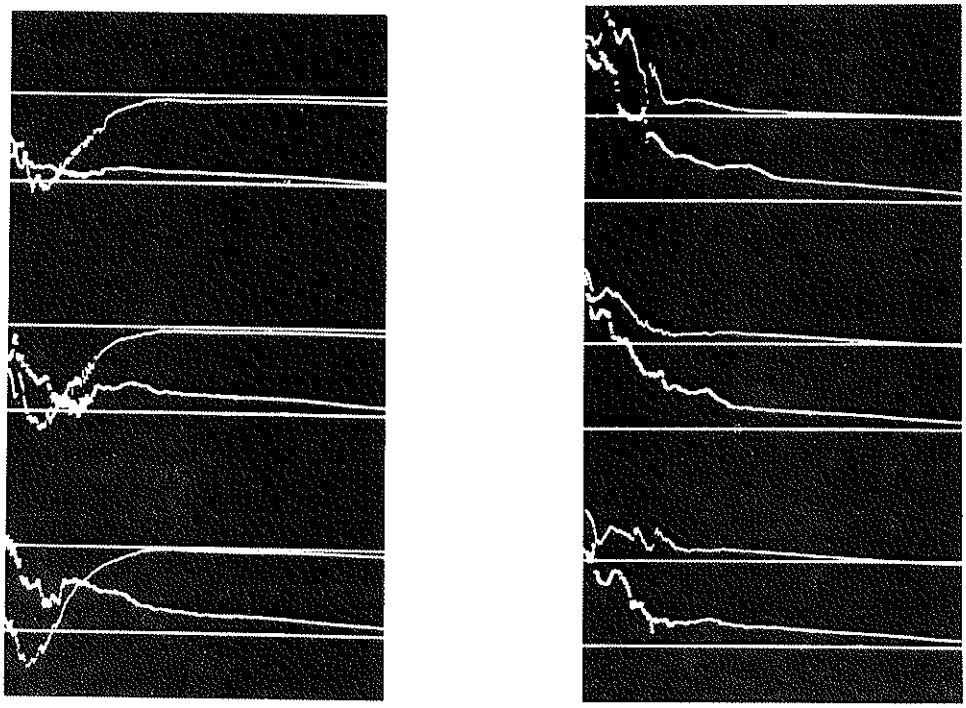

A B

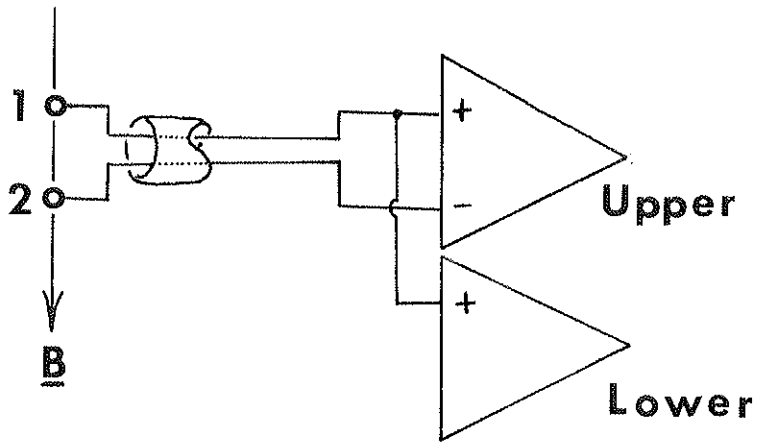

C

(vi) Vacuum Cleanable and Expandable Probes

A special design was developed for probes meant to acquire quantitatively trustworthy data. From the above observations, this requires that the tip be perfectly clean when the data are taken. Due to previous usage, however, the quarter inch probe ports typically have their channels coated with vacuum grease which collects dust and grit. No probe may be guaranteed clean after insertion. Electron bombardment of tips prior to insertion into other devices has proven[14] to be an effective cleaning technique since the ports could be maintained clean. Figure 9 illustrates how this technique was adapted to clean a probe tip inside the octupole vacuum chamber. Construction details are available elsewhere[15] but in general the probe has a filament mounted at the end of a sliding narrow tube and inserted into a stainless probe body next to the platinum tip. The vacuum seal is made at the air end of the probe body. After the probe is inserted into the chamber, the filament is moved near the tip and heated with a 6 V power supply. The tip is biased to +400 V and draws several hundred milliamperes of electron current. When used in a glass test chamber, the tips glowed white hot. A 10 sec heating pulse has proven to be sufficient to allow the pressure gauge of the small test chamber to return to normal. The filament is pulled back from the tip into the end of the probe body and the data is taken. When used in the gettering region, this should be done every hour or so.

The debye length, λ_d, in the low density, hot plasma varies from half to one millimeter. A double probe should have its tips 5 to 10 λ_d apart to properly isolate the tips. A one centimeter separation was

Figure II 9

Diagram of a self cleaning probe.

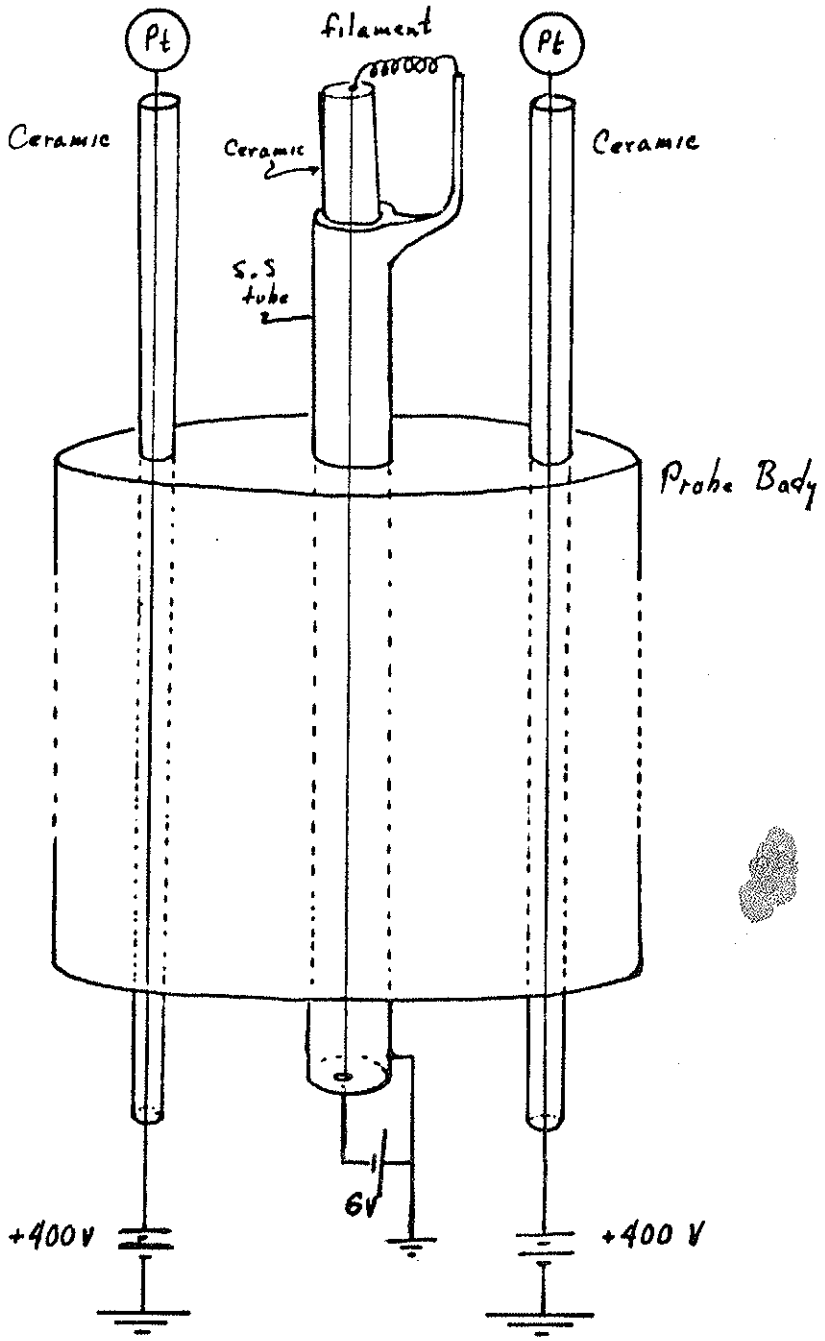
Pt
filament
Pt
Ceramic
Ceramic
Ceramic
S.S
tube
Probe Body
6V
+400V
+400 V

chosen as a safe value and proved to be useful for fluctuation measurements but posed a problem since the ports are only 1/4" in diameter. Figure 10 is a photograph of a typical probe which solves the problem. Each platinum tip is part of a type 2 probe stem. The small tube has a double bend in it at the main stainless probe body and extends through spacers in the body, through the compressed viton pad at the air end and out into the laboratory. The small tubes may be rotated nearly 180° from the deployed position shown to the closed position with the small tips less than 1/4" apart. When the cleaning filament (not shown) is included in the unit, the entire self-cleaning expandable double probe will fit through the air lock. Figure 11 is a photograph of the main probe used to acquire the levitated data in Chapter III.

B: Acquisition Techniques

The majority of the results presented in this thesis require the systematic processing of a great many data records. Figure 12 shows a block diagram of the basic elements needed for computer management of the acquisition and analysis of data. The computer used is a Digital Equipment Corporation PDP-11/20 with 28 K, 16 bit words. The differential input analog-to-digital (A/D) signal converters used are three Biomation 610-B 6 bit, 256 word transient recorders and one Biomation 610 6 Bit, 128 word unit. These units are capable of digitizing at a 10 MHz rate and are synchronized to a common clock. The signal comes from the probe and is processed by the "probe box" which represents the electronic processing performed on the signal before it reaches the oscilloscope. The oscilloscope amplifier displays the transient signal

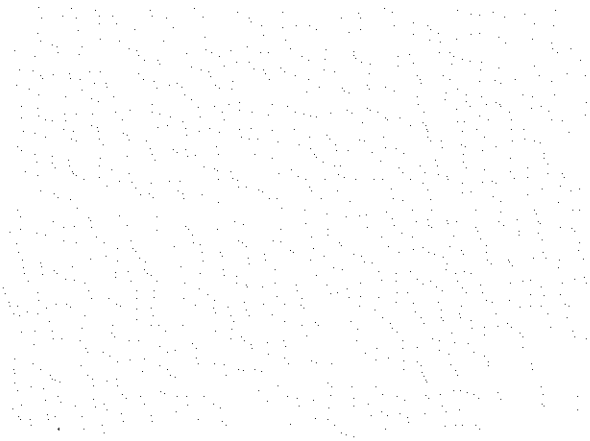

Figure II 10

Photographs of an expandable probe designed to acquire data for $\psi > \psi_s$ in the bridge. (A) Tip design, (B) The vacuum seal is made using a Cajon fitting at the air end of the probe.

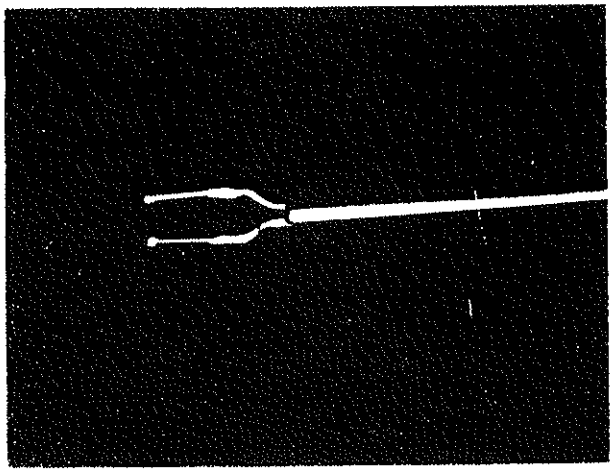

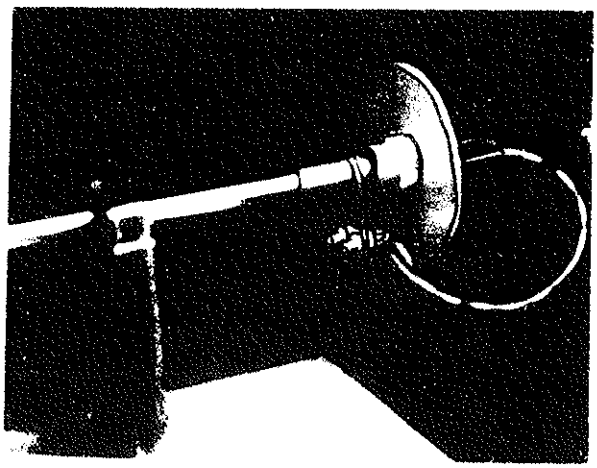

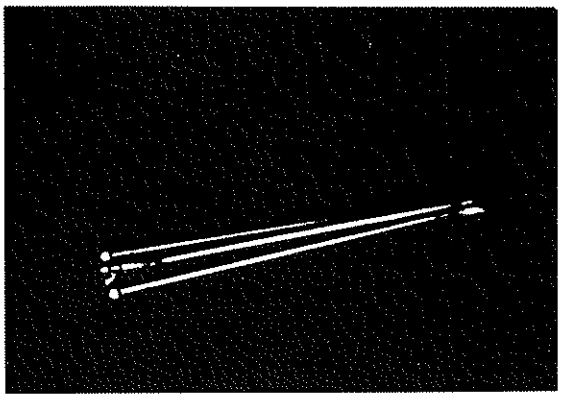

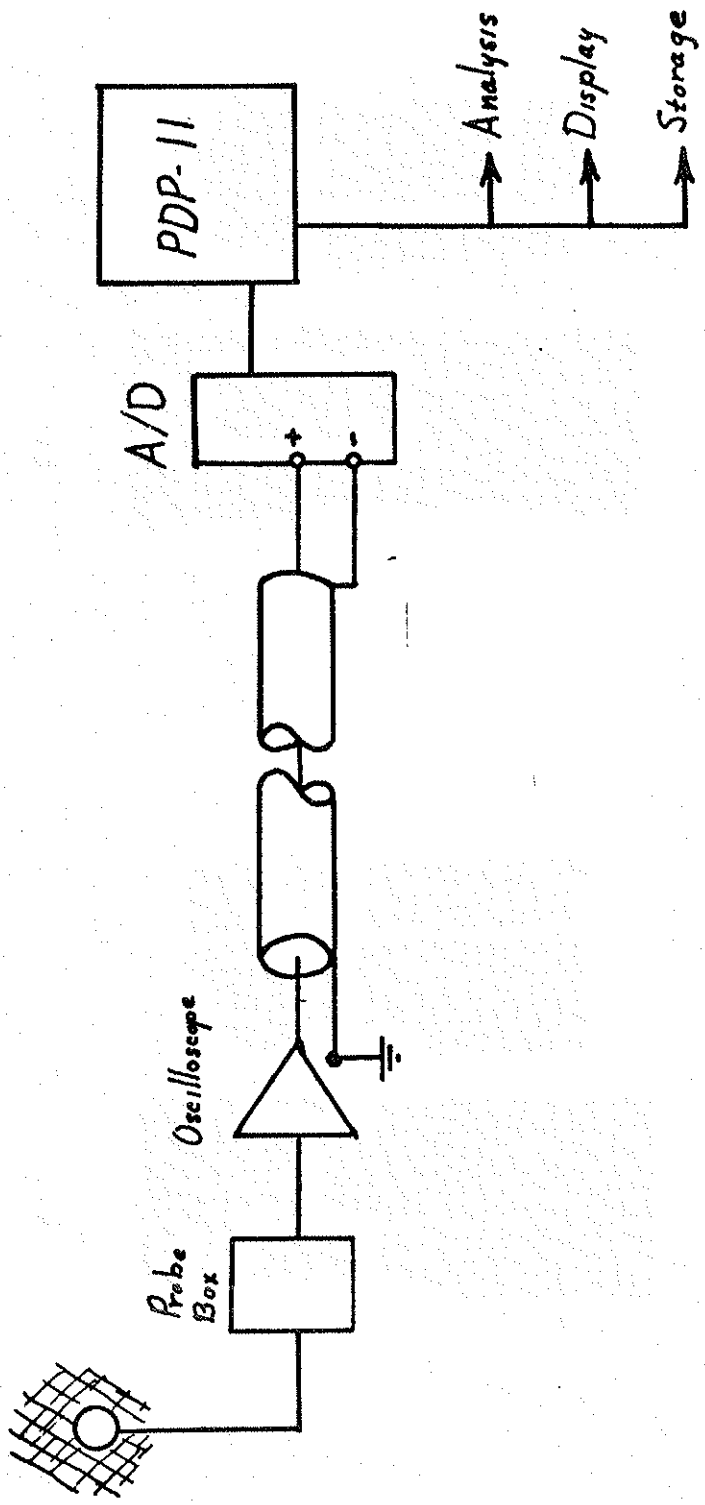
PDP-11
Analysis
Display
Storage
A/D
+
-
Oscilloscope
Probe Box

Figure II 12

Block diagram of the computer acquisition system.

Figure II 13

Comparison of data from an oscilloscope with its digitized image.

(A) Oscilloscope record: 1 V/div, 2 msec full scale horizontal sweep.

(B) Digitized image of A: 1.42 V/div, 2.56 msec full scale.

(C) Oscilloscope record: 1 V/div, 2 msec full scale horizontal sweep.

(D) Digitized image of B: 1.10 V/div, 2.56 msec full scale.

on its screen and drives it down the RG-62/U cable to the A/D station. The A/D is triggered once per machine pulse and the digitized data are read by the computer[16] after each pulse.

The primary purpose of the computer is to acquire the data records and save them on paper tape for subsequent analysis. The time between octupole pulses is adequate, however, for most analytical purposes. The software I have written to acquire and analyze the data is called DATANAL and is described elsewhere.[17] At present, DATANAL is capable of acquiring, saving, and displaying the data, and, within a few additional seconds, finding (i) the least squares best fit to the data, (ii) the correlation function[18] between various data records, (iii) the Fourier transform of the data, and (iv) various other matrix operations useful in acquiring and analyzing data. Figure 13 shows a signal taken directly from the oscilloscope and its digitized image as acquired and displayed by the computer.

C: Profile Acquisition

As used in this thesis, a "profile" is any plot of data versus some parameter fixed throughout the pulse. Examples of such profiles are the graphs of floating potential from a probe versus position in the machine as seen in Figures III 8-13 and graphs of current drawn to a probe tip versus the bias on that tip. This latter type of profile has been used with DATANAL to get I-V plots for a probe in order to obtain computer measurements of T_e.

Figures I 6 and III 7 show a number of shots in the levitated octupole to demonstrate the problems involved in constructing a reason-

able profile. Two major problems are evident: (i) fluctuations or noise in the data signal, and (ii) shot-to-shot irreproducibility in the signal for the same profile parameter. The problems caused by (i) arise, for example, when one wishes to discover the bulk, "zeroth order," distribution and temporal evolution of some property, such as density or potential. This fluctuational uncertainty may be relieved by averaging the signal over a time interval which includes fluctuation periods. The inverse problem arises when the object of the study is the fluctuations themselves, as in subsection D. Problem (ii) may sometimes be helped by using a monitor probe and standardizing the data magnitude with it.

To get a better idea of what is happening, let the data be represented as $d_k(\underline{x},t)$ for the k-th machine pulse at position $\underline{x}$ and time t. Suppose d_k may be written as

$$d_k(\underline{x},t) = D_k\ P(\underline{x},t) + \delta_k(\underline{x},T_o,t) \qquad \text{[II-C-1]}$$

where $P(\underline{x},t)$ is the physical profile shape factor, D_k is the data amplitude which depends on such pulse parameters as the filling density or temperature. The fluctuating part of the data is $\delta_k(\underline{x},T_o,t)$ where T_o is the longest characteristic time of the oscillations. In the following paragraphs, three separate methods are discussed for making the profile independent of the per shot variability of the plasma.

(i) Interval Averaging

We might define δ as being the portion left over after d_k has been averaged over a time $T_d >> T_o$:

$$\delta_k(\underline{x}, T_o, t) = d_k(\underline{x}, t) - \frac{1}{T_d} \int_{t - T_d/2}^{t + T_d/2} ds\ d_k(\underline{x}, s) \qquad [II\text{-}C\text{-}2]$$

If $P(\underline{x}, t)$ changes appreciably in the time T_d (as it might) this is not satisfactory. A better method would be to curve fit a low order polynomial, $\bar{d}_k$, to the data in the interval and subtract that from the data. For a given position $\underline{x}$,

$$\bar{d}_k(\underline{x}, t) = \sum_{j=0}^{M} C_j(\underline{x})\ t^j \qquad [II\text{-}C\text{-}3]$$

$$\delta_k(\underline{x}, T_o, t) = d_k(\underline{x}, t) - \bar{d}_k(\underline{x}, t). \qquad [II\text{-}C\text{-}4]$$

The $\{C_j\}$ are the coefficients of the least squares best fit polynomial of order M defined in the interval $(t - T_d/2,\ t + T_d/2)$. The l.s.b.f. polynomial should be used because the δ_k defined by [4] has a zero average in the T_d interval. Notice that if M = 0, [2] and [4] are identical. DATANAL uses the third order l.s.b.f. polynomial from subroutine CURVE for the values of $\{C_j\}$. In other words, the fluctuations may be practically removed by using $\bar{d}_k$ instead of d_k. Then [1] will be replaced by

$$\bar{d}_k(\underline{x}, t) = D_k\ P(\underline{x}, t) \qquad [II\text{-}C\text{-}5]$$

with $\bar{d}_k$ found by [3].

(ii) Reference Scaling

The shot-to-shot variations in D_k may frequently be removed by

standardizing the signal of [1] or [5] with the signal from a data monitor whose profile parameters (such as position, impedance, bias, etc.) are not changed on any shot. This reference monitor is assumed to generate data of the same type as the data which are being profiled. On a given shot, the reference monitor data will also obey [5]:

$$\bar{d}_k^{(r)} = D_k \, P^{(r)}(\underline{x},t) \qquad \text{[II-C-6]}$$

The idea is to have previously averaged $\bar{d}_k^{(r)}$ over a number of shots and to have obtained $<d^{(r)}>$:

$$<d^{(r)}(\underline{x},t)> = \sum_{k=1}^{N} \bar{d}_k^{(r)}/N = <D> \, P^{(r)}(\underline{x},t). \qquad \text{[II-C-7]}$$

Now, on the k-th pulse, we can multiply [5] by $<d^{(r)}>$ and divide by $\bar{d}_k^{(r)}$ and get, using [5, 6 and 7]

$$<d(\underline{x},t)> = <D> \, P(\underline{x},t). \qquad \text{[II-C-8]}$$

This is the pulse independent zeroth order profile of the data d.

It is easy to misuse reference scaling. For example, the average amplitude for the floating potential, $<V_f>$, and for the ion saturation current, $<I_s>$, can not be the same quantities. I_s data must not be scaled by a V_f monitor because [8] would give a meaningless answer. The same applies to scaling I_s fluctuations with an I_s profile monitor, and so forth. In fact, fluctuation data should be reference scaled only by a fluctuation monitor of the same type. All of these will destabilize the data profiles being constructed. In fact, it is questionable whether V_f may be reference scaled at all, since V_f is the sum

of the plasma space potential and a term proportional to the electron temperature. If there is shot-to-shot variation in T_e, temperature gradients, or if T_e decays at a different rate than V_p then reference scaling must not be used. The rule to use is that data may only be standardized by a like-type reference monitor. Even then, if the k-th pulse's monitor varies too much from its average value, the physics might change and change the data profile factor $P(\underline{x},t)$. It is a good second rule to always print out $(d_k^{(r)} - \langle d^{(r)} \rangle)/\langle d^{(r)} \rangle$ so that the pulse may be ignored if it is too far out of range. When applicable, however, reference scaling can be invaluable in smoothing profile data. It has significantly smoothed density profiles, I-V probe characteristics, and r.m.s. fluctuation amplitudes of both potential and density versus position. In the data reported in the later chapters, a ±15% acceptance interval was used whenever possible.

(iii) Pulse Averaging

Both of the averaging processes represented by equations [3] and [8] may be done quickly by the computer between shots and involve no additional effort by the experimenter. (The experimenter must initially find $\langle d \rangle$ by [7] but the number of shots need not be very large.) However, it is frequently impossible to completely average out the δ_k because it is impractical to set $T_d >> T_o$. In that case both [5] and [8] have a small added fluctuating term which will affect the profile analysis. (Note that no assumption of smallness is made in [1].) If the result of [8] is averaged over several (K) pulses, the fluctuating component will (usually) phase mix to zero. The final profile, then,

is

$$d(\underline{x},t) = \underbrace{\frac{1}{K}\sum_{k=1}^{K}}_{\text{pulse avg.}} \underbrace{\frac{\langle d^{(r)}\rangle}{\bar{d}_k^{(r)}}}_{\text{reference scaling}} \underbrace{\left[\sum_{j=0}^{M} C_j(\underline{x};k)\, t^j\right]}_{\text{interval average}} \qquad \text{[II-C-9]}$$

D: Fluctuation Acquisition and Analysis

The problem divides into two parts: (i) identification of the fluctuation component from the slowly varying "zeroth order" bulk portion of the data, and (ii) analysis of the data using correlation and Fourier transform techniques.

(i) Normalization of Fluctuation Data

As indicated in subsection C, any data signal is composed of a part which varies rapidly in time, and an offset which has a much slower variation, see [II-C-1]. The process of removing the slowly varying component from the fluctuating signal is consistently called "normalization" throughout this thesis. Although it is somewhat arbitrary how the two components should be separated, the choices available to the experimenter will make major differences in fluctuational quantities such as r.m.s amplitudes. It is important that the normalization method, once chosen, be applied consistently to all the data analyzed. For all the data presented here, the fluctuation is what is left after the time average of the signal is removed. This zero average property is the proper choice for the quantities used in the particle transport studies of Chapter V. The turbulence studies of Chapter IV will show that an amplitude offset is generated which might cause

interpretation problems. However, there is no clearly defined prescription for uniquely identifying a random turbulence signal so the above definition is still applied.

Using the notation of subsection C, let $d_k(\underline{x},t)$ be the input data signal. This signal might well have been processed by an electronic filter with a "D.C." offset added by the filters, line drivers, etc. The fluctuation component of d_k will be written (following [II-C-4] as $\delta_k(\underline{x},T_o,t)$ where

$$\delta_k(\underline{x},T_o,t) = d_k(\underline{x},t) - \overline{d}_k(\underline{x},t) \qquad \text{[II-D-1]}$$

where $\overline{d}_k$ has the property of being the time average in some manner of d_k over an interval T_d which is much greater than T_o, the longest time variation of δ_k. Following the argument after [II-C-2], $\overline{d}_k$ is not just the simple average of d_k. δ_k ultimately is to be time correlated and Fourier transformed in order to obtain all of the information available. As described in the following paragraphs, the correlation function retains all of the Fourier components of the original data and any slow time variation not removed from d_k will appear in the Fourier spectrum and quite possibly dominate it. Figures 14-16 show the effect of a "D.C." ramp and offset on the analysis of a fluctuation data record. If the ramp and offset are too large they will obscure the fluctuation analysis. For this reason, DATANAL (ref. Section II-B), uses the least squares best fit of an order M polynomial for $\overline{d}_k$ in equation [1]. If $M=0$, $\overline{d}_k$ is the simple average of d_k and any zero frequency offset will be removed. An $M=1$ fit would in addition remove a linear ramp, and an $M=2$ fit would remove a constant curvature in

Figure II 14

(A) Data trace as acquired by the computer.

(B) The same trace after the best fit linear function has been subtracted. Both data are .96 msec long and the vertical units are 59.6 mV per inch.

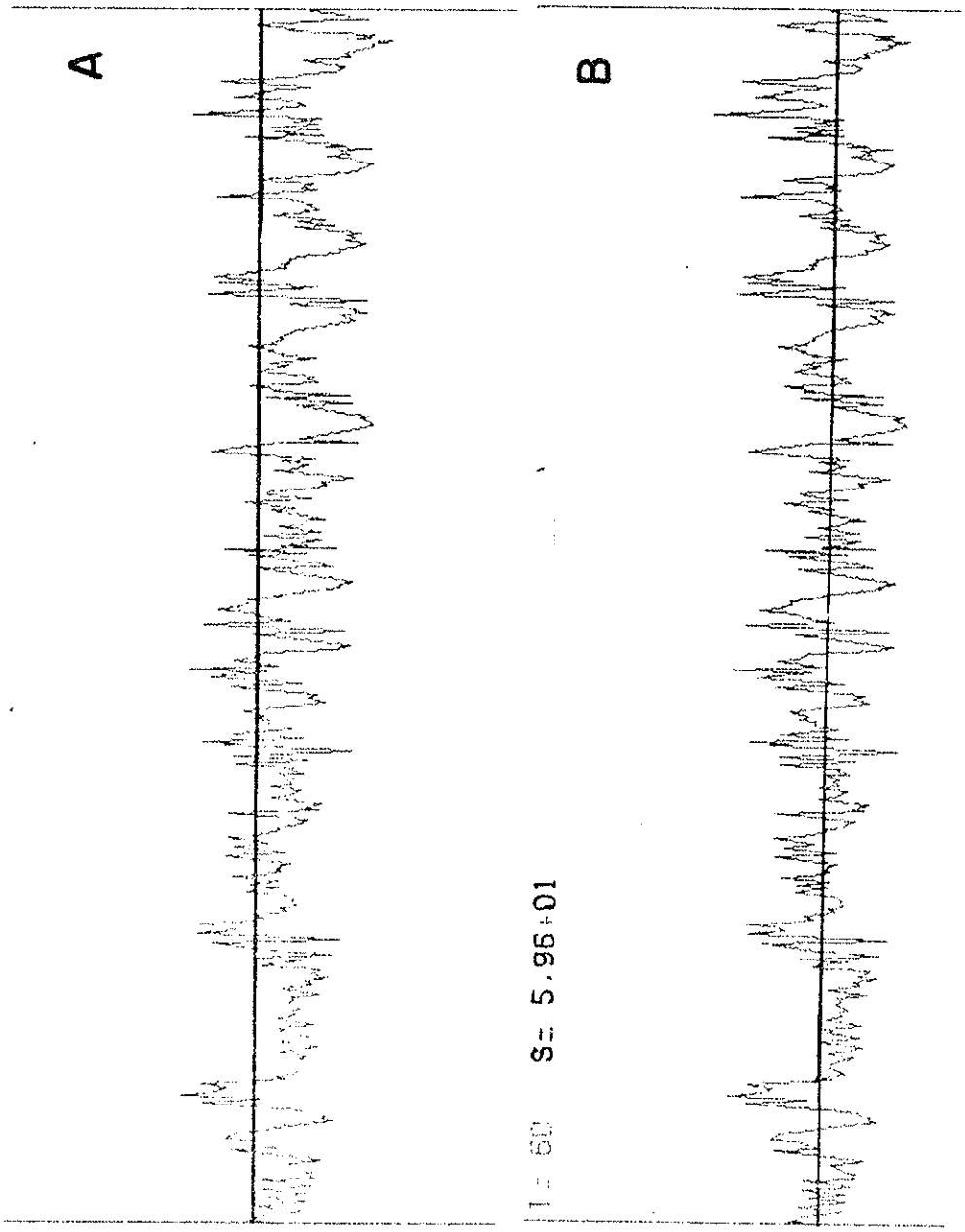
A
B
S= 5.96+01

Figure II 15

(A) Auto correlation function of 14 A.

(B) Auto correlation function of 14 B.

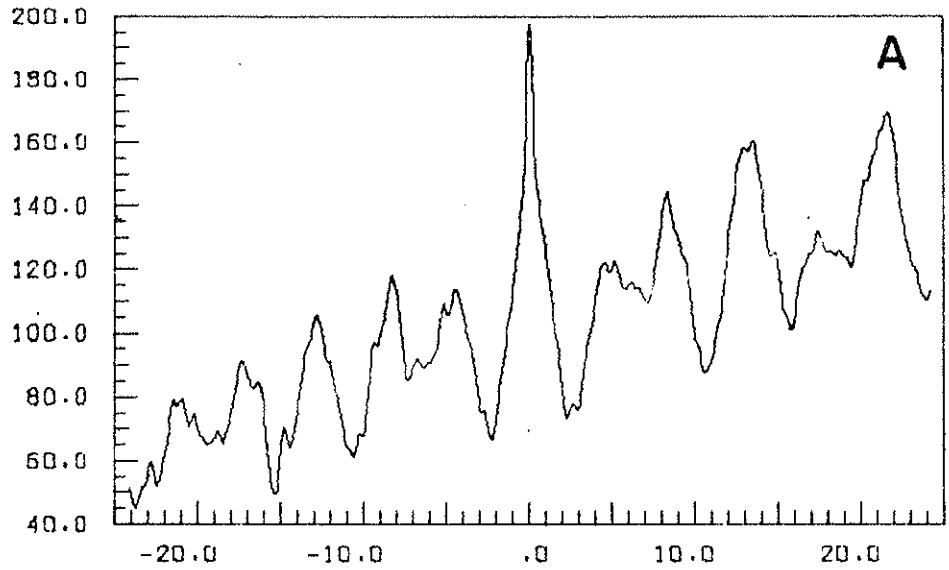
200.0
180.0
160.0
140.0
120.0
100.0
80.0
60.0
40.0
-20.0
-10.0
.0
10.0
20.0
A

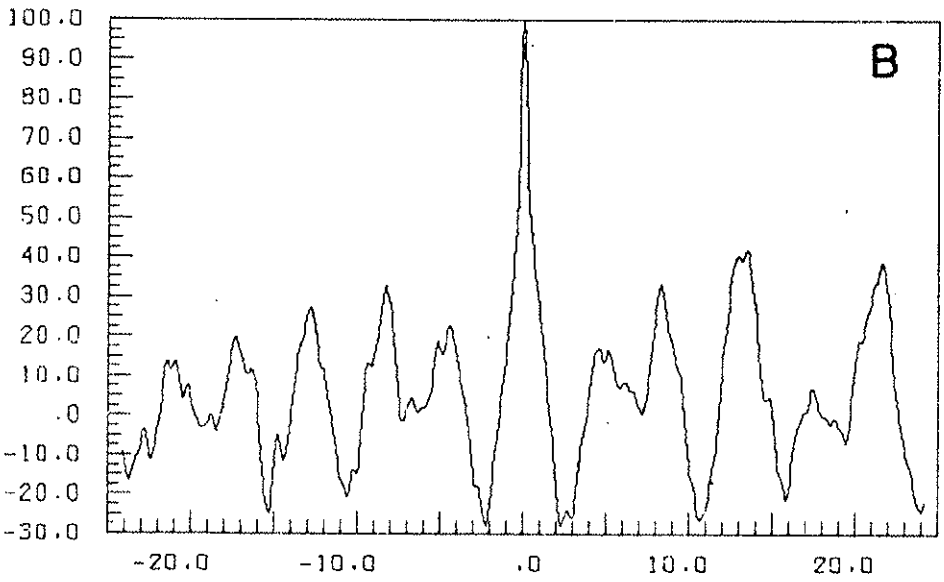
100.0
90.0
80.0
70.0
60.0
50.0
40.0
30.0
20.0
10.0
.0
-10.0
-20.0
-30.0
-20.0
-10.0
.0
10.0
20.0
B

Figure II 16

(A) Real part of the Fourier transform of 15 A.

(B) Same for 15 B. The low f component implies that a second or third order function should have been used to normalize 14 A.

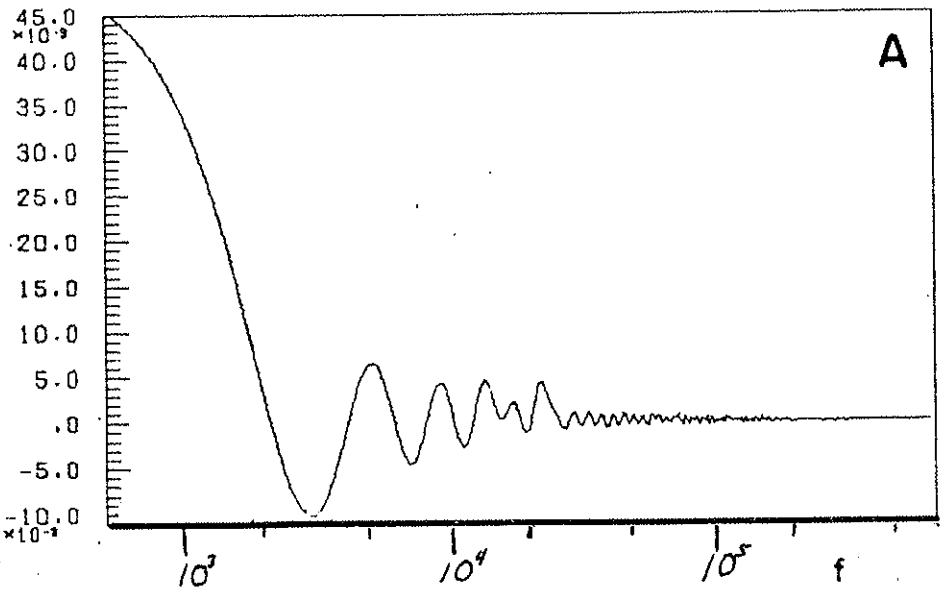
45.0
×10⁻⁹
40.0
35.0
30.0
25.0
20.0
15.0
10.0
5.0
.0
-5.0
-10.0
×10⁻⁹
10³
10⁴
10⁵
f
A

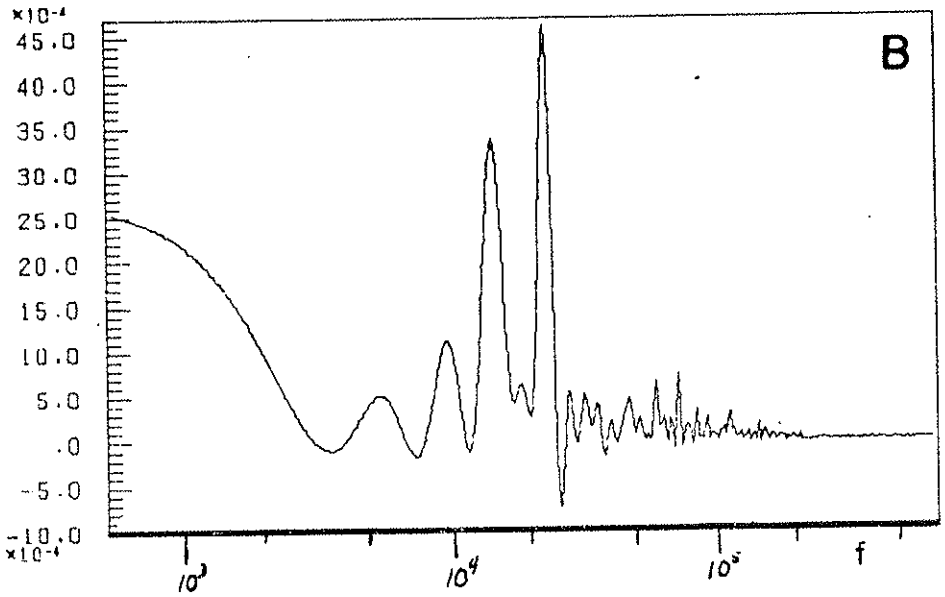
×10⁻⁴
45.0
40.0
35.0
30.0
25.0
20.0
15.0
10.0
5.0
.0
-5.0
-10.0
×10⁻⁴
10³
10⁴
10⁵
f
B

that ramp. Since M = 3 essentially removes a single oscillation period from the data, it is obvious that high order M must be used only with great care if the fluctuation to be analyzed are not themselves to be damaged. For example, suppose the input data is 256 μsec long and has had all frequencies below 10 kHz electronically filtered from it. An M = 3 curve fit would numerically remove all frequencies present below 5 kHz and is therefore not an unreasonable normalization. As explained below, good numerical calculation of a correlation function requires that eight to ten cycles of the fluctuation be present in the data record. For this case, the M = 3 normalization should offer no problem in data destruction.

(ii) Analysis of Fluctuation Data

The principal information desired from any fluctuation data are the average amplitude of the signal, its characteristic times and lengths, and its relative motion with respect to the observer. The data are said to be coherent if the Fourier spectrum is sharply peaked in time and space and to be turbulent if it is not.

For coherent data with well-defined oscillations, this information set is the period and wavelength of the oscillations averaged over time and distance intervals which are long with respect to their averaged values. In addition, the coherence (correlation) time and length of the signal is needed as a measure of the rate at which the period and wavelength change. The phase velocity of the signal is the ratio of the wavelength to the period.

For turbulence data, the relevant information is the lifetime

(correlation time) and velocity of each characteristic spatial length in the signal. The observer also needs the average rate at which the probe encounters each turbulence length in the signal. This indicates whether the turbulence occurs in well separated bursts and is spatially and temporally isolated, or whether it is dense, with the occurrence of the turbulence signals overlapping in time and space. In practice, it is very difficult to obtain this entire set of information.

If the data are oscillations at a single pure frequency, then direct inspection of the data record itself will yield all the necessary information without further analytic effort. Unfortunately, most plasma data usually indicate the presence of multiple coherent frequencies, of random variations (for even a single frequency component) of the frequency, phase and amplitude, or of a dominant non-coherent turbulence component. In these cases, the required information may be extracted from the data by first finding the auto or cross correlations of the data record with itself or similar records, and then Fourier transforming that function in time or space. The correlation function will be defined below. Its purpose is to ensemble average random quantities in the manner to be described. The amplitude, frequency and phase of the signal may then be found from the Fourier transform. It should be noted that this is not the order in which such calculations are occasionally performed.[19,20] The reason for the present method is that the Fourier transform is a stochastic function and is susceptible to noise, whereas the correlation function is not. This point will be further discussed at the end of this section.

The following six paragraphs define the correlation function and

its response to various sorts of randomness in the input data. Since the first five points to be discussed have been considered in detail in PLP-480, the pertinent problems and principal results will be merely sketched here.

1. The Correlation Function: Let $F_1(t,z_o)$ and $F_2(t,z_o+z)$ be two data records which have been obtained between the times t_1 and t_2 and at the positions z_o and z_o+z. The correlation function in time and space $C(F_1,F_2;\tau;z)$ is defined as[21,22,23]

$$C(F_1F_2;\tau;z) = \frac{1}{T_o}\int_{\bar{t}-T_o/2}^{\bar{t}+T_o/2} F_1(t,z_o)\ F_2(t+\tau,z_o+z)\ dt \qquad \text{[II-D-2]}$$

where $\bar{t} = (t_1+t_2)/2$ and T_o is the integration time interval. The relative time shift τ between F_1 and F_2 ranges between $\pm\tau_m$ where, if the data time interval $T_D = t_2 - t_1$, $\tau_m = (T_D - T_o)/2 > 0$. The theoretical correlation function is the limit of C as T_o approaches infinity. The convolution, $\bar{C}$, is defined as $\bar{C} = T_oC$ in [2], or, to be precise, as the limit as T_o grows without bounds. The correlation C of coherent oscillations is a finite number, whereas $\bar{C}$ is infinite. However, C is zero for a single non-repeated "blip," whereas $\bar{C}$ has a finite value. Notice that [2] does not perform a direct spatial averaging of the data. For steady state ("stationary") fluctuations, the best definition of the correlation function is the ensemble average of the shifted product of two data records. For this type of data, the time average of [2] is equivalent to an ensemble average and the above definition of C is correct. However, C is actually independent of $\bar{t}$ and z_o only for

stationary data. For nonstationary data, even the concept of frequency runs into problems[24] unless the time variations are "slow." See paragraph (2), below.

If F_1 and F_2 may be Fourier decomposed as $F_1(t) = \Sigma\ F_{1k}\ \cos(\omega_k t)$, $F_2(t) = \Sigma\ F_{2k}\ \cos(\omega_k t + \phi_k)$, then

$$C(F_1,F_2;\tau) = \Sigma(F_{1k}F_{2k}/2)(\cos[\omega_k\tau + \phi_k] + er_k). \qquad [II\text{-}D\text{-}3]$$

If the error term er_k is negligible, each component reaches its maximum value at $\tau_k = -\phi_k/\omega_k$. An important theorem is that

$$C(F_1,F_2;\tau) = C(F_2,F_1;-\tau). \qquad [II\text{-}D\text{-}4]$$

(a) The error term may be shown to be $\leq 1/(\omega_k T_o)$. To keep this term relatively small, T_o should be eight to ten times larger than the longest period in the data train. This, of course, reduces the significance of the error only for the extrema of the k-th component; the zero of that component is poorly calculated.

(b) Fortunately, there is a second method of reducing the error. It may be shown that er_k is proportional to sine functions of the phase of F_1 and F_2 with respect to t_1, the beginning of the data record. If C is calculated for N different data records and averaged together to form $\langle C\rangle = \Sigma C_j/N$, er_k will phase average to zero no matter what $\omega_k T_o$ is. Since this averaging procedure is equivalent to ensemble averaging, $\langle C\rangle$ is always the quantity that should be used whenever possible. This is not always experimentally feasible, however. Small shot-to-shot changes in the plasma parameters may place the fluctuation on significantly different points of its dispersion curve with each

machine pulse, and a sequence of shots will trace out that region of the dispersion relation. <C> can not be formed and accuracy may be obtained only through the use of long data records. The BIOMATION 610-B A/D transient recorder described in section B is barely adequate for the requirements if accuracy in both phase and frequency is desired.

2. Coherent Signals With Slow Frequency Change: Consider a single component of [3] only. Suppose that the frequency for F_1 is $\omega(1;t) = \omega_o + \omega_1(t - \bar{t})$ where ω_o is the instantaneous frequency at the middle of the data record. F_2 is the same as F_1 but shifted in time by τ_o. That is, $F_2(t)$ has for its frequency $\omega(2;t) = \omega_o + (t - \bar{t} - \tau_o)$. It is straightforward to show that the correlation function for this component is

$$C(F_1,F_2;\tau) = \left[\frac{F_1F_2}{2}\cos(\omega_o\tau)\right]\frac{\sin(\omega_1T_o\Delta\tau)}{\omega_1T_o\Delta\tau} \qquad \text{[II-D-5]}$$

with $\Delta\tau = \tau - \tau_o$ and $\omega = \omega_o + \omega_1(\tau - \tau_o)$. The term in square brackets is the expected C for a signal with a constant frequency ω_o since $\phi = -\omega_o\tau_o$ is the phase given by [3]. If the integration time T_o is very large, C approaches a delta function at $\tau = \tau_o$. Figure 17 shows an example of this for data from the octupole. The plasma was injected 5 msec after the start of the multipole field and the data is taken 5 msec later (43° into the sine pulse). Notice that the diffraction envelope of [5] changes signs at $\tau = \tau_o \pm \pi/\omega_1T_o$. This well accounts for the otherwise puzzling effect that the amplitude of C first decreased

Figure II 17

(A) Two data records, 871 and 872, which show the effect of a slowly increasing frequency.

(B) The cross correlation between the two records. Notice the phase inversion at $\tau = -3.5 \times 10^{-4}$ and $+2.5 \times 10^{-4}$ sec.

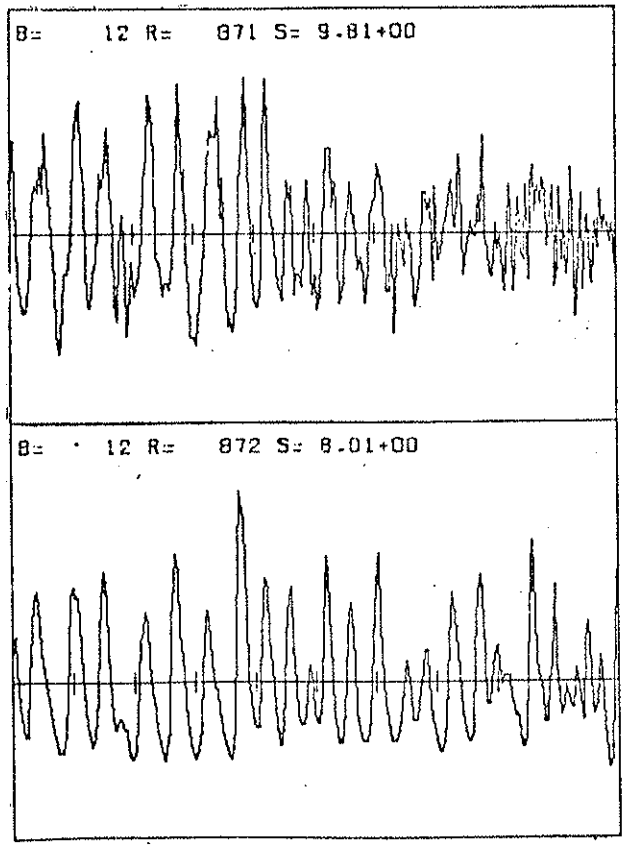

A

C(871, 872) BATCH(12, 12)

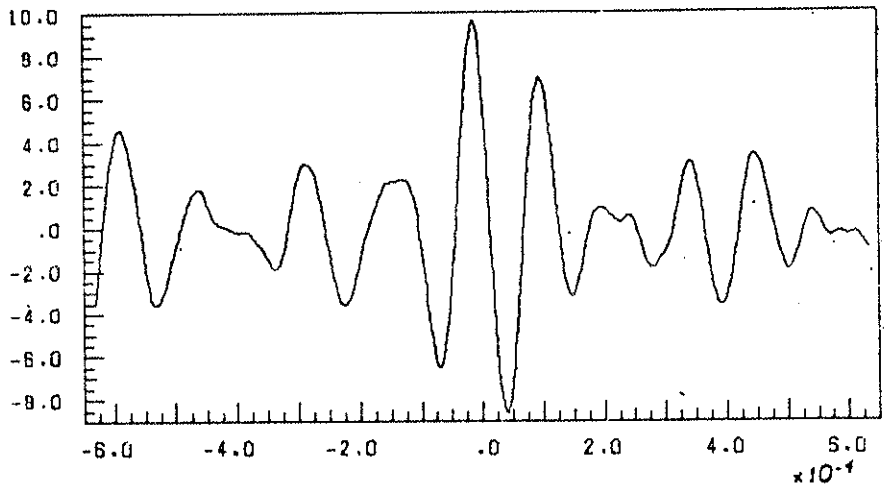

B

to a minimum then increases again, and that the phase of C apparently changes at the minimum.

3. Coherent Signals With Random Frequency Variations: On an oscillation-to-oscillation basis, the period of a fluctuation usually varies randomly about some average value $2\pi/\omega_o$. This turbulence in frequency is averaged by C if the data interval is large enough so that the integration samples the ensemble of all probable frequencies, or if C is averaged over many separate pulses to achieve the same ensemble averaging. If the sample length is too small then C for a single shot is quite sensitive to the turbulence. In order to calculate this effect, assume that the probability that at time t the frequency is in the interval $(\omega,\omega+d\omega)$ is $N \exp[-(\omega-\omega_o)^2/2\sigma^2]\, d\omega$. The average frequency is ω_o, N is the unity normalization constant and σ is the frequency variance (r.m.s. deviation of ω from ω_o). The problem naturally divides into two subparts depending on whether the turbulent signal is the same for F_2 as for F_1 but shifted by τ_o, or whether the turbulence in F_2 is independent of F_1.

(a) Shared turbulence: Auto correlations fall under this category. If $F_2(t)$ is just $F_1(t)$ shifted by τ_o then each component of [3] becomes

$$\langle C(F_1,F_2;\tau)\rangle = \left[\frac{F_1F_2}{2}\cos(\omega_o\Delta\tau)\right] \exp\left[\frac{-\sigma^2}{2}\Delta\tau^2\right] \qquad \text{[II-D-6]}$$

where, again, $\tau_o = -\phi/\omega_o$.

(b) Unshared turbulence: F_1 and F_2 are averaged over the ensemble separately and, for $\sigma T_o \gg 1$, $\Delta\tau \ll T_o$:

$$<C(F_1,F_2;\tau) = \left[\frac{F_1F_2}{2}\cos(\omega_o\Delta\tau)\right]\frac{\sqrt{\pi}}{\sigma T_o}\exp\left[\frac{-\sigma^2}{r}\Delta\tau^2\right] \qquad \text{[II-D-7]}$$

It is easy to mistake the exponential envelope of [6] or [7] with the "diffraction" envelope of [5]. C must extend far enough in τ to assure that the cosine amplitude does not increase again.

4. Coherent Signals With Randomness In Amplitude: Suppose that the Fourier amplitudes of F_1 and F_2 are random functions of time but that the frequency is constant. Then [3] becomes

$$C(F_1,F_2;\tau) = \sum_k \left[\frac{\int F_{1k}(t)F_{2k}(t+\tau)\,dt}{T_o}\right]\frac{\cos(\omega_k\tau+\phi_k)}{2} \quad . \qquad \text{[II-D-8]}$$

The amplitude of C is just the average of the product of the correlation time shifted amplitudes. If the average is performed over too small a sample, the non-regular amplitudes can exaggerate or depress the net amplitude of C. Figure 18 shows an example of this accidental enhancement of the correlation peaks. The integration time for C is half the data record and for F_1 is centered in the middle of the record as shown by the dotted box. The integration window for F_2 is time shifted through the entire record. When the window is shifted as shown by the dotted box, the indicated data peaks overlap and enhance the marked correlation peak. There are at least three ways to avoide this problem. The input records may be very large, sometimes a difficult problem for a pulsed device.[25] The correlation function may be calculated twice and [4] used to form the net C:

Figure II 18

Two data records are shown in (A) which lead to the heightened peak in (B) which is marked by an arrow. The integration intervals in the records which are used to form the correlation function are shown for $\tau = 0$ by dotted lines. When $\tau = 15 \times 10^{-5}$ sec, the peak indicated by the arrow in 131 overlaps the indicated peak in 132. The data is actually well correlated near $\tau = 0$ as may be visually confirmed by viewing the data from the bottom of the page, at a shallow angle.

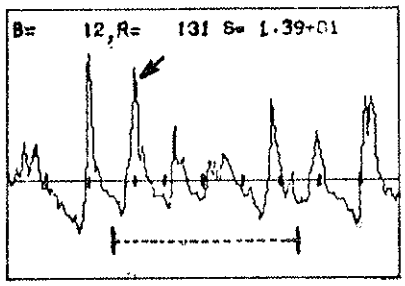

A

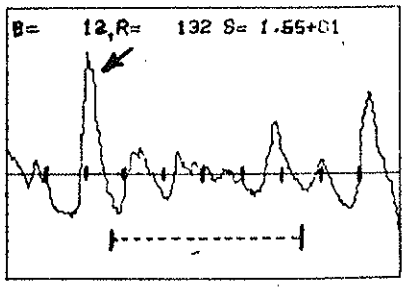

.C(131, 132) BATCH(12, 12)

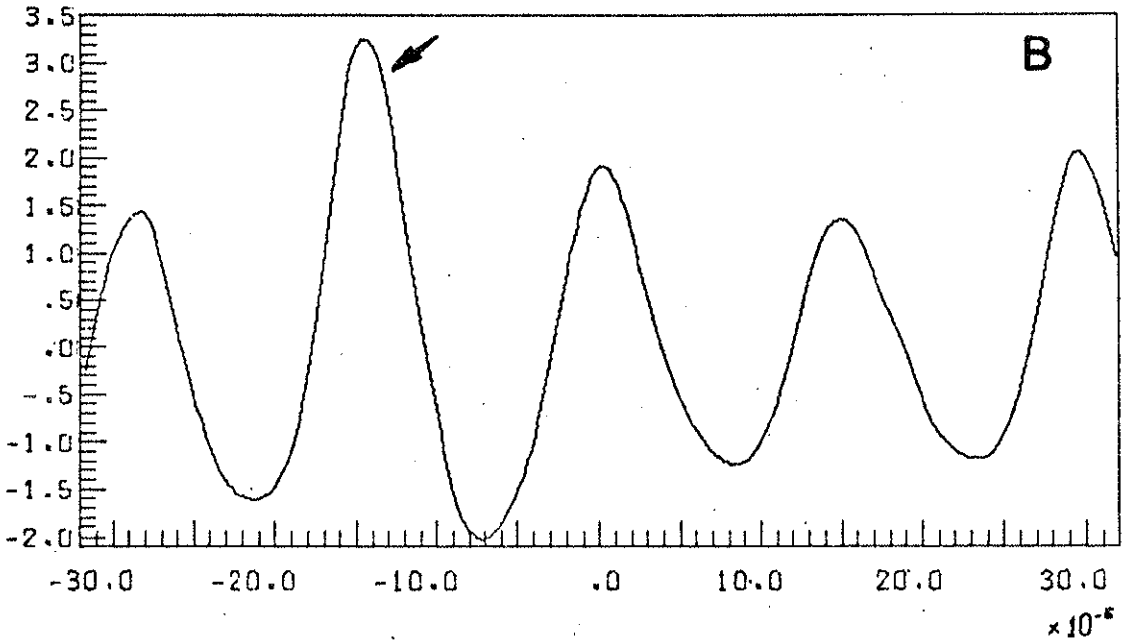

$$C(F_1,F_2;\tau) = \frac{1}{2}[C(F_1,F_2;\tau) + C(F_2,F_1;-\tau)]. \qquad [II\text{-}D\text{-}9]$$

In addition, the net C used may be the average of the C calculations for many successive shots.

5. Rapid Random Turbulence: Suppose incoherent spikes appear in the data with no apparent time width. This is the appearance of turbulence with lifetimes shorter than the data sampling period. Suppose that the probability that the amplitude is between $(a,a+da)$ is $N \exp(-a^2/2A^2)$. This assumes that the average amplitude of the noise is zero. The noise correlation is a spike whose amplitude is A^2 which is added to the coherent C at $\tau = \tau_o$.

6. Random Turbulence Of Arbitrary Lifetime: This is a much more serious problem than that posed by the preceding paragraph because the entire central peak of C will be modified. Discussion of this, however, will be delayed until Chapter IV where the analysis techniques for turbulence are presented along with the results of the investigation.

(iii) Correlation v.s. Fourier Transform

It is occasionally stated[21,26] that the correlation function (CF) and Fourier transform (FT) are completely equivalent functions: the CF defined over the time-space domain, and the FT defined over the frequency : wave-vector domain. This is due to a misusage of the Wiener-Khintchine theorem[27] for the case of turbulent signals as has been discussed elsewhere.[28] Physically, however, the differences in stability to randomness in data may be readily understood. The CF is a sequence of the time averages of the product of two data records. Each

value in the sequence is the average of a different time shift between these records. For staionary data, this is equivalent to ensemble averaging. The FT, however, is a curve fitting routine. It has been shown[29] that the Fourier integral is the amplitude which provides the least squares best fit of a sinusoid to a data train. Thus, if the signal is sufficiently turbulent and lasts for a finite length of time, the algorithm will fit a frequency component with non-zero amplitude to the noise. This situation is a turbulence generalization of the usual[26] process of aliasing, which means curve fitting a non-existent high (finite) frequency component to a low (zero) frequency component which has not been sampled sufficiently often.

Interpretation of an FT is also complicated by the phenomenon of "leakage." Even for a pure frequency in a finite data record, the structure of the FT amplitude in frequency is the same as the diffraction structure in space of a pure frequency passing through a single slit. There exist large side lobes to the pattern which make resolution of different frequencies quite difficult. People who apply the FT to data[20] usually multiply the data by an artificial amplitude function which suppresses the side lobes. However, when the FT is applied to the CF of data with turbulence, the turbulence itself has modified the amplitude of the coherent component (see [5], [6], and [7]) in a manner similar to the Hanning amplitude popularly used[26] to suppress leakage. In principle, one could measure the strength of the turbulence by comparing the size of the side lobes with the diffraction amplitude expected, although in practice this is usually very difficult. Figure 19 A, B, C, and D show a data record, its auto CF and the comparison

Figure II 19 A,B

A data trace is shown in (A) and its auto CF in (B).

Figure II 19 C,D

The FT of B is shown in C and the two frequencies are well isolated. The FT of the data in A is shown in D, which is the real component of the complex FT.

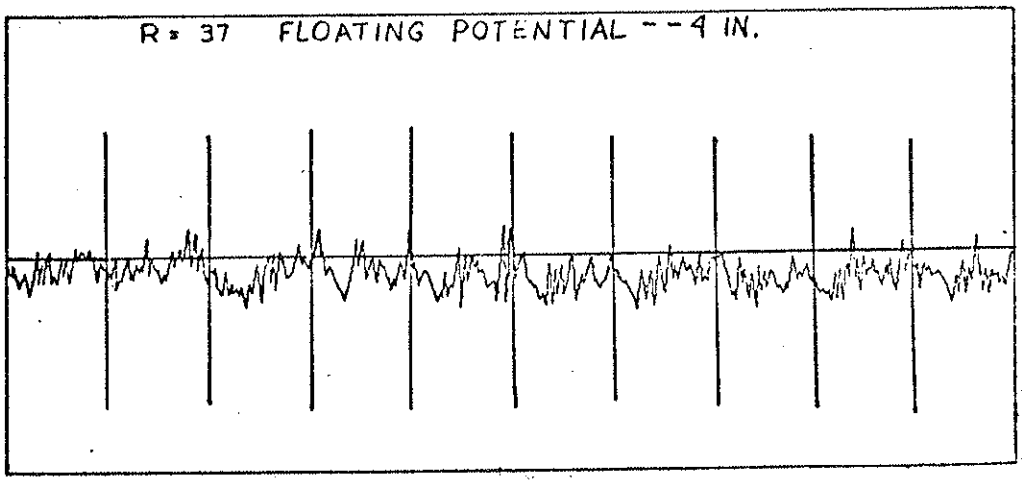
R = 37 FLOATING POTENTIAL -- 4 IN.

19 A

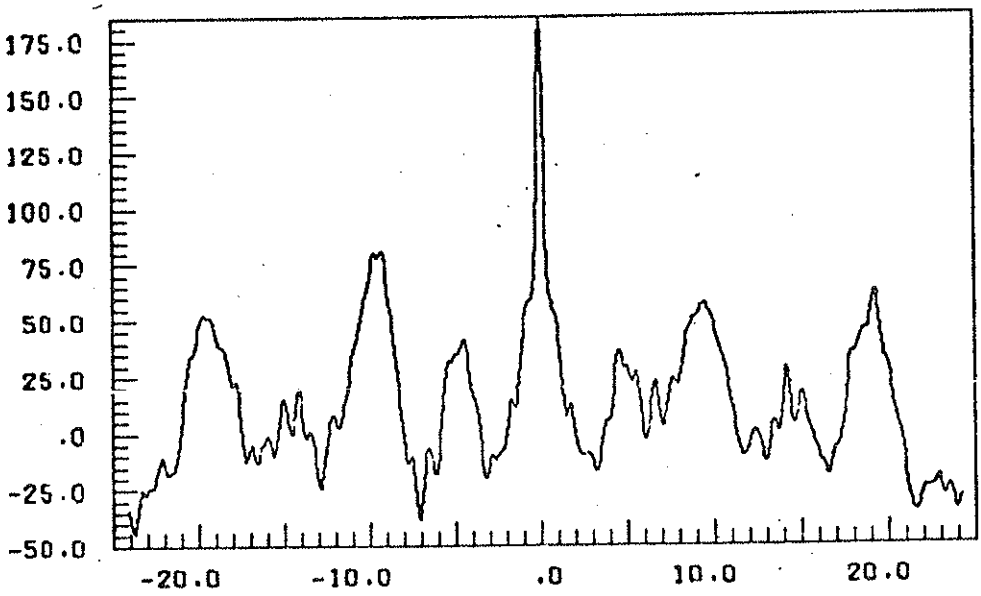
175.0
150.0
125.0
100.0
75.0
50.0
25.0
.0
-25.0
-50.0
-20.0
-10.0
.0
10.0
20.0

19 B

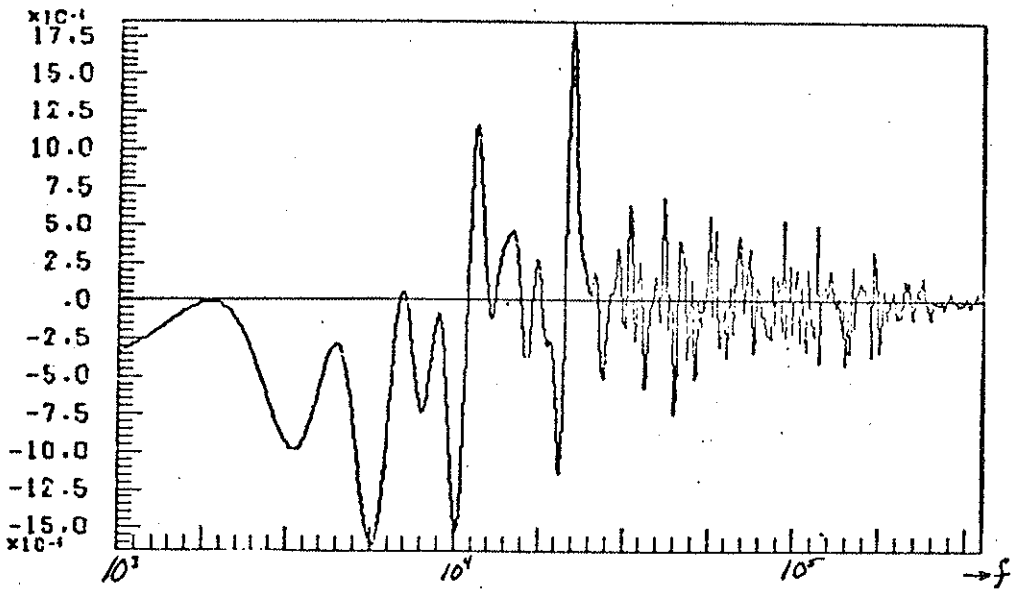
×10⁻⁴
17.5
15.0
12.5
10.0
7.5
5.0
2.5
.0
-2.5
-5.0
-7.5
-10.0
-12.5
-15.0
×10⁻⁴
10³
10⁴
10⁵
→f

19 C

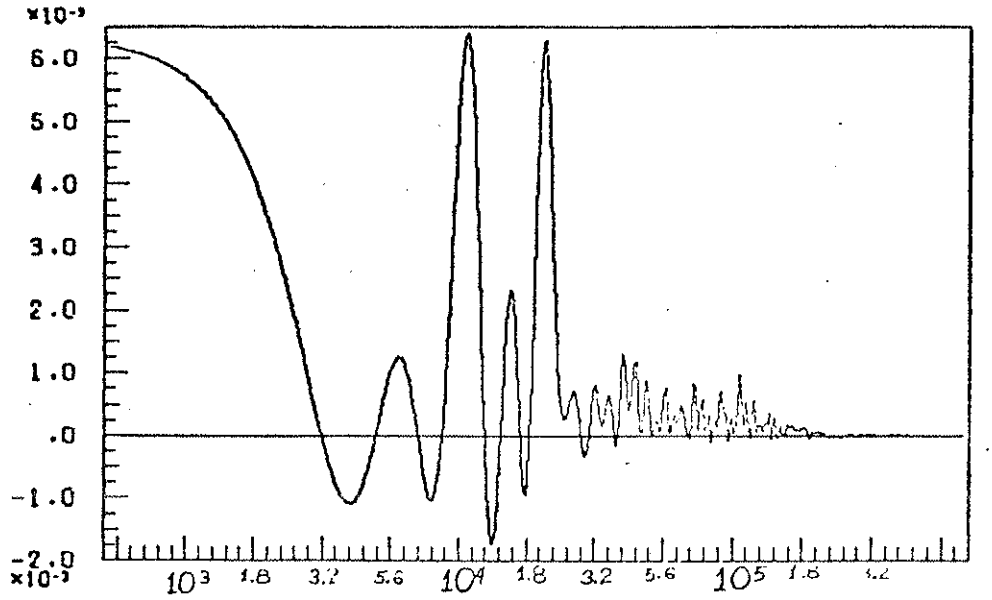
×10⁻³
6.0
5.0
4.0
3.0
2.0
1.0
.0
-1.0
-2.0
×10⁻³
10³
1.8
3.2
5.6
10⁴
1.8
3.2
5.6
10⁵

19 D

between the FT of the raw data and the FT of the CF. The CF-FT sequence is much easier to interpret than the direct FT of data.

In summary, then, the Data-CF-FT sequence is the one which should be used since the ensemble averaging of the CF will stabilize the resulting FT. In addition, the FT will retain the phase information contained in [3]. The FT for a given component may be written as $A \exp(i \phi_k)$ and A^2 may be found from the power spectrum which is the sum of the squares of the real (Re) and imaginary (Im) components. The phase angle is $\phi_k = \tan^{-1}(\mathrm{Im}/\mathrm{Re})$ at the peaks in the power spectrum. The information from the FT will be the best fit A, ϕ, and ω from the entire CF, whereas these can be extracted from the CF alone only at the central peak and therefore with a high degree of error. The value normally[21] called the "power spectrum" is the real component of the FT of the auto CF of data. In general, this value is $(\mathrm{Re}^2 + \mathrm{Im}^2)^{1/2}$ at the peak in the usual power spectrum.

REFERENCES FOR CHAPTER II

1. F. F. Chen. Plasma Diagnostic Techniques, R. H. Huddelstone, S. L. Leonard, ed. (Academic Press, N. Y., 1965) p. 113

2. J. C. Sprott, University of Wisconsin Plasma Physics PLP-88

3. R. K. Richards. Ph.D. Thesis. University of Wisconsin (1976)

4. W. Lochte-Holtgreuen, ed. Plasma Diagnostics (Wiley Interscience, N. Y., 1968)

5. J. C. Sprott. Review of Scientific Instruments 37, 897 (1966)

6. J. G. LaFramboise. UTIAS No. 100 (University of Toronto, Toronto, 1966)

7. J, R. Sanmartin. Phys. Fluids 13, 103 (1970)

8. J. S. Chang, J. G. LaFramboise. Phys. Fluids 19, 25 (1976)

9. J. W. Rudmin. J. Appl. Phys. 47, 4833 (1976)

10. J. R. Drake, J. R. Greenwood, G. A. Navratil, R. S. Post. Phys. Fluids 20, 148 (1977)

11. J. R. Greenwood. Ph.D. Thesis, University of Wisconsin (1975)

12. E. O. Johnson, L. Malter. Phys. Rev. 80, 58 (1950)

13. The following papers have treated the problems of V_f or I_s measurements.
    V_f measurement problems are presented in the following two papers:
    J. C. Sprott, D. E. Lencioni, J. A. Schmidt. PLP-135 (1967)
    J. C. Sprott. PLP-175 (1968)
    Explanations attempted in the following problems:
    G. L. Schmidt. PLP-292 (1969) Problem solved by heating tips.
    G. W. Kuswa. Ph.D. Thesis (1970) Explanation of problem due to work function of tip material.
    I_s problems due to surface contaminates were seen by
    J. Barter. PLP-521 (1973)
    J. W. Rudmin. J. Appl. Phys. 47, 4833 (1976)

14. W. C. Guss. Ph.D. Thesis. University of Wisconsin (1976)

15. C, J. Armentrout. University of Wisconsin Plasma Physics PLP-727

16. M. C. Zarnstorff, J. R. Greenwood. Bul. Am. Phys. Soc. 21, 1080 (1976)

17. C. J. Armentrout. University of Wisconsin Plasma Physics PLP-481

18. C. J. Armentrout. University of Wisconsin Plasma Physics PLP-480

19. D. E. Smith, E. J. Powers, G. S. Caldwell. IEEE Transactions on Plasma Science PS-2, 261 (1974)

20. Y. Amagishi. Institute of Plasma Physics Technical Report IPPJ-T-26 (1976)

21. G. Bekefi. Radiation Processes In Plasmas (John Wiley & Sons, Inc., N. Y., 1966)

22. I. P. Shkarofsky. Proceedings on the Symposium on Turbulence of Fluids and Plasmas. XVIII (Polytechnique Press, Polytechnique Institute of Brooklyn, N. Y., 1968) p. 289

23. E. B. Hooper. Plasma Physics 13, 1 (1971)

24. L. Mandel. Am. J. Phys. 42, 840 (1974)

25. J. A. Schmidt. Ph.D. Thesis. University of Wisconsin (1975)

26. E. O. Brigham. The Fast Fourier Transform (Prentice-Hall, Inc., Englewood Cliffs, N. Y. 1974)

27. N. Wiener. Acta Math. 55, 117 (1930)

28. C. J. Armentrout, K. R. Symon. University of Wisconsin Plasma Physics PLP-726

29. G. Birkhoff, G.-C Rota. Ordinary Differential Equations (Blaisdell Publishing Company, Waltham, Mass., 1962) Ch. XI

CHAPTER III: BULK PROPERTIES OF THE PLASMA

A: Temperature Measurements

(i) The Electron Temperature

The electron temperature, T_e, has been measured using the technique[1] of sweeping the bias of a Langmuir probe (single tipped, low impedance ... see II A) from a negative value of 3 ... 5 T_e below V_f to a positive voltage of about the same amount. If the bias sweeps through its full range much faster than the plasma properties change, then the operating point of the probe will move along the probe's characteristic curve of Figure II 2(b). By sweeping the probe linearly in time, the probe characteristic may be displayed on an oscilloscope screen or digitized by a transient recorder. However, there are two principal difficulties with this scheme.

Firstly, one can not usually place the entire characteristic on a screen or in a 6 bit digitizer and retain the accuracy in the ion saturation branch needed for the processing described below. This is because the ratio of electron to ion saturation currents is the ratio of electron thermal speed to ion sound speed[2] which for $T_i \leq T_e$ is $(m_i/m_e)^{1/2} \cong 42$. One must usually be content to display the curve from deep into ion "saturation" to somewhere near V_p. Figure III 1(a) shows this data and its ramp for plasma at ψ_s.

Secondly, one may not be allowed to sweep the probe fast enough. Fluctuations occur at the edges of the plasma (near the rings and walls) where the density is quite low. These are waves with between

10 and 30 kHz frequencies and an r.m.s. amplitude between 20 and 50% the time averaged density. On the other hand, at these low densities, the plasma frequency is on the order of a megahertz. Symon has shown[3] that as a signal changes on times approaching $1/f_p$, the debye length expands without bounds and a signal at $1/f_p$ would drive all the plasma on the flux shell (assuming density is constant on the shell). The ramp, then, should be quicker than 10 μsec to be "much faster" than the changing plasma density, but should last longer than 10 μsec to be "much slower" than $1/f_p$. Figure 1(b) shows one of the worst cases where the 100 μsec ramp is in a roughly 30 kHz wave near ψ_c. Nevertheless, the main body of the plasma is much higher in density and quieter and the swept probe measurements yield reasonable values.

Figure 2 shows the circuit used to generate the ramp. The ammeter is the same as in Figure II 5. Most advanced probe theories which account for sheath expansion with probe bias (section II A) predict that for potentials below V_p, the current drawn may be written as approximately

$$I(V) = I_{io}(V) - I_{eo}\exp[(V - V_p)/T_e] \qquad \text{[III-A-1]}$$

$$I_{io}(V) = I_o + I_1(V_f - V) \qquad \text{[III-A-2]}$$

where V is the (negative) tip bias and ion current is assumed to be positive. I_o is the ion current drawn at $V = V_f$ when the net current drawn is zero. The proper technique is to fit $I_{io}(v)$ to the ion saturation branch, subtract it from the total current everywhere below V_p, and plot $\ln[I(V) - I_{io}(V)]$ versus V to get T_e from the inverse of the

Figure III 1

Swept probe traces for T_e measurement. The period of the sweep is 100 μsec and the bias voltage (ramp trace) changes from -45 V to +45 V.

(A) Three successive shots of ψ_s, 30 msec into field pulse, and 5 msec after injection.

(B) Three shots at 8 cm in the lower outer bridge region.

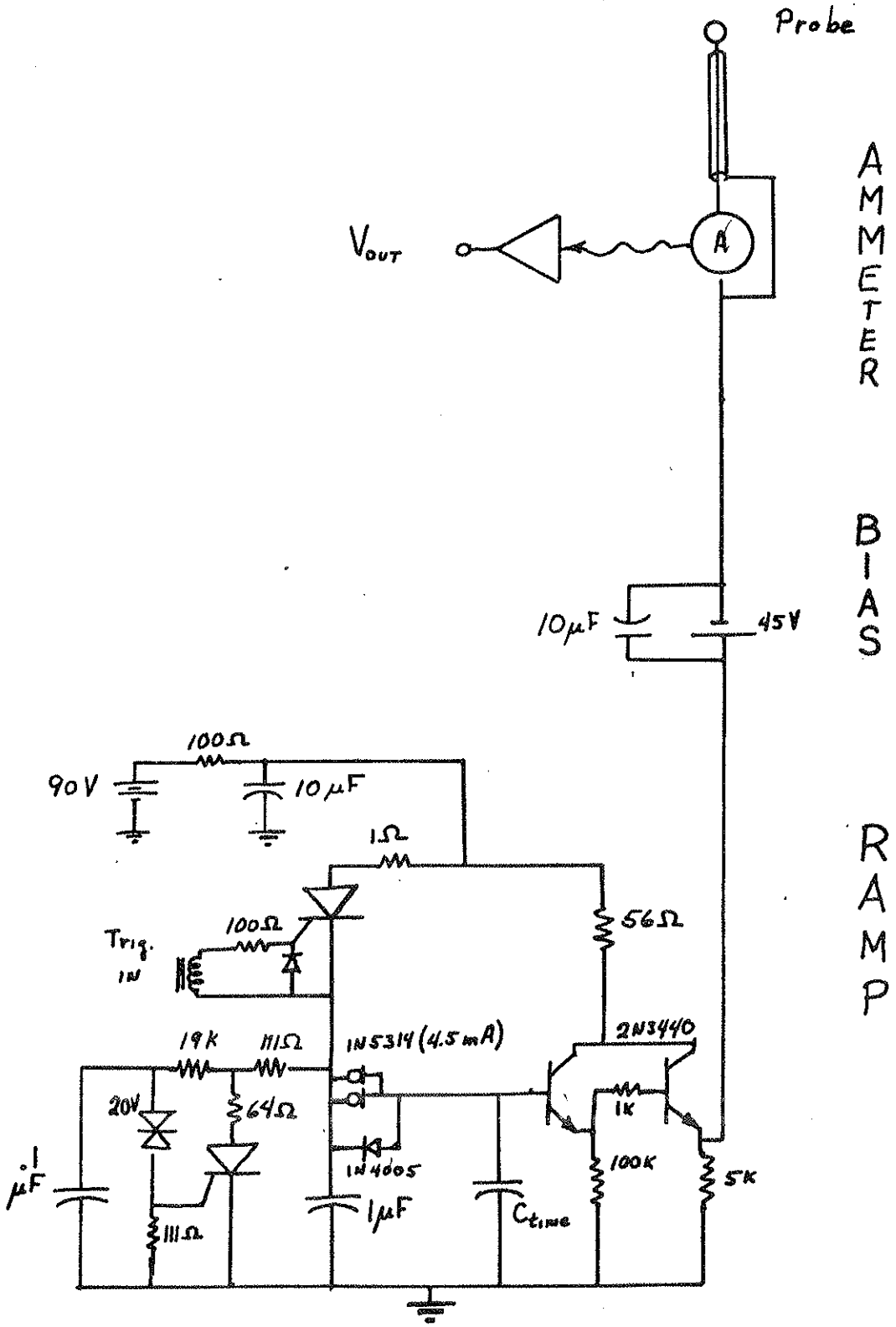
Probe
AMMETER
V_{OUT}
A
BIAS
10μF
45V
RAMP
100Ω
90V
10μF
1Ω
56Ω
100Ω
Trig. IN
19K
111Ω
1N5314 (4.5mA)
2N3440
20V
64Ω
1K
1N4005
100K
5K
1μF
111Ω
C_{time}

slope. E. J. Strait is currently developing a program for the PDP-11 system to curve fit a line and an exponential from entire characteristic simultaneously in order to obtain unambiguously the coefficients I_o, I_1, I_{eo}, and T_e^{-1}. In the future, the best way to measure T_e from probe characteristics will be to abandon the sweeping circuitry and acquire the current : bias curve on a point by point basis as in Figure II 6 and apply the curve fitting routine. Using the considerations of Chapter II C, rapid time variations in the data need not disturb the accuracy of the resulting temperatures. Another advantage to this is that T_e as a function of time is obtained automatically.

The results of swept probe measurements are shown in Figures 3 and 4 for gun plasmas in the poloidal field octupole with the normal operating pressure. The results were summarized in Table I 2. There is no significant difference between the levitated and supported ring cases for either T_e or $\tau_{Te} = - T_e/\dot{T}_e$. Figure 5 shows T_e as a function of position along the mid cylinder from the wall to a point inside ψ_c. The points were obtained by overlaying a number of curves similar to Figure 1(b) and visually tracing the most reasonable characteristic curve. This was done a number of times for each position and the scatter is fairly large. However, the mean value for T_e joins well with the values of Figures 3 and 4 which supports the contention that $\nabla T_e = 0$ in the machine. This spatial uniformity is attributable to the turbulent injection and capture process that accompanies gun generated plasmas.[4] These data, along with the spot checked observations elsewhere in the device by the author and others, suggest that the behavior of T_e is essentially independent of a wide range of machine parameters.

Figure III 3

T_e for the hydrogen plasma as a function of position in lower outer bridge and of time. Rings levitated and the background pressure is 2×10^{-7} Torr. V_c = 2.5 kV, crowbarred field.

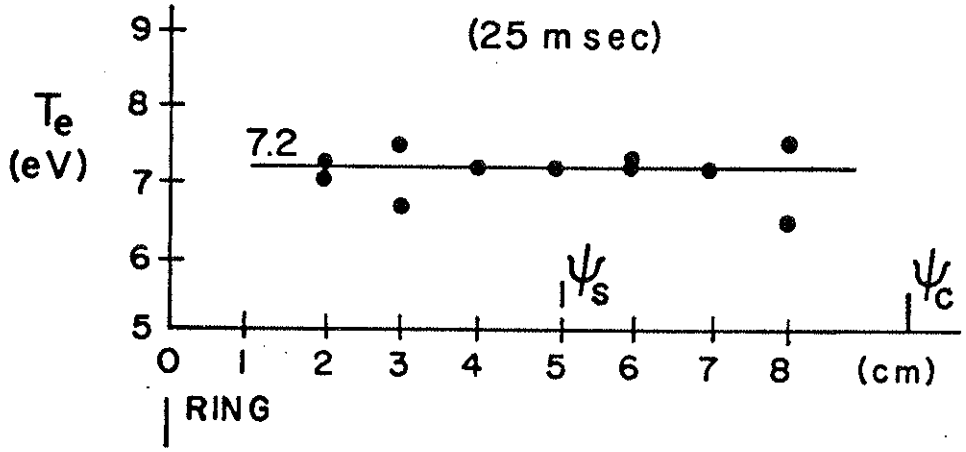
(25 m sec)
T_e
(eV)
9
8
7
6
5
7.2
ψ_s
ψ_c
0
1
2
3
4
5
6
7
8
(cm)
RING

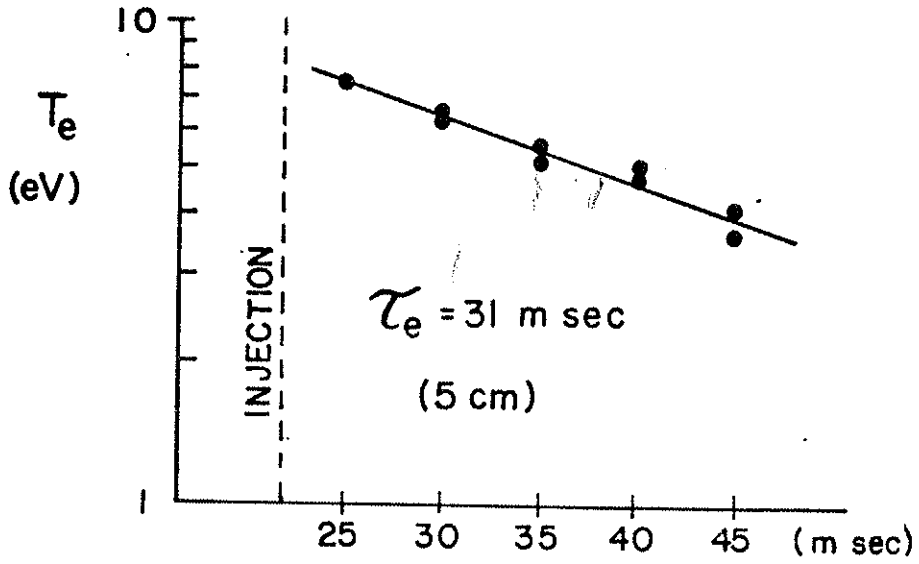
10
T_e
(eV)
1
INJECTION
τ_e = 31 m sec
(5 cm)
25
30
35
40
45
(m sec)

Figure III 4

T_e for same operating conditions as 3, but with rings supported.

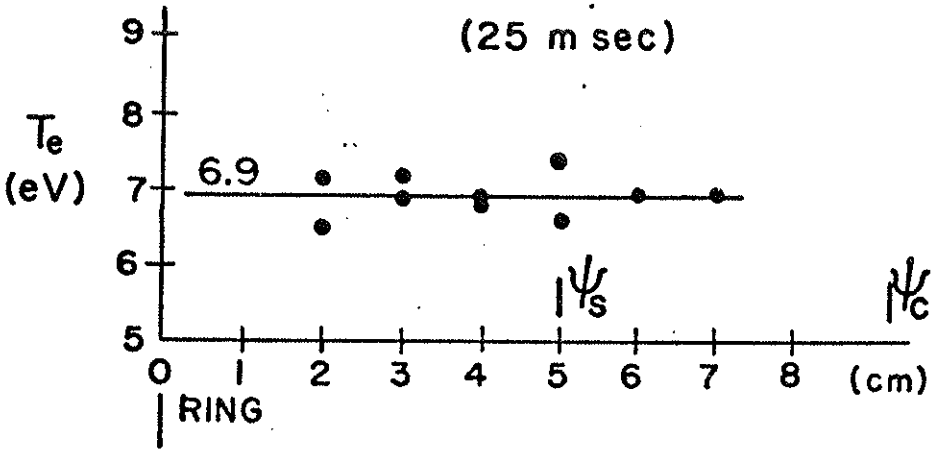
(25 m sec)
T_e
(eV)
9
8
7
6
5
6.9
ψ_s
ψ_c
0
1
2
3
4
5
6
7
8
(cm)
RING

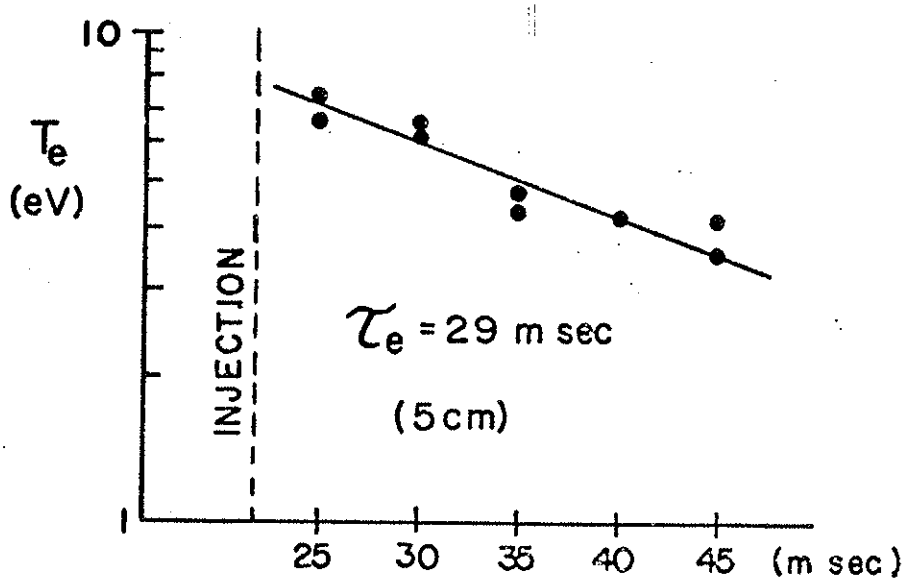
10
T_e
(eV)
1
INJECTION
τ_e = 29 m sec
(5cm)
25
30
35
40
45
(m sec)

Figure III 5

T_e 5 msec after injection along the mid cylinder.

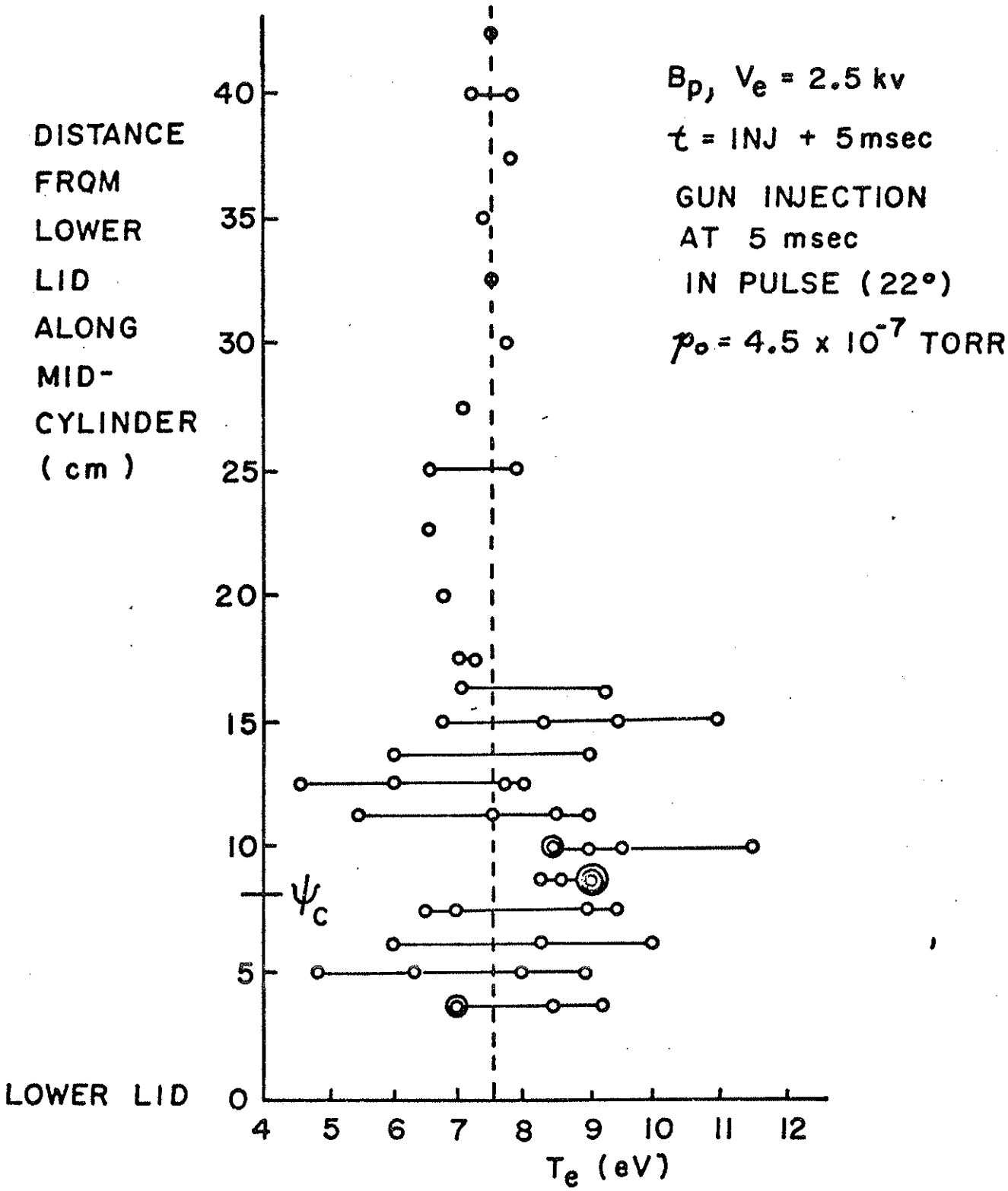
DISTANCE FROM LOWER LID ALONG MID-CYLINDER (cm)
40
35
30
25
20
15
10
5
0
LOWER LID
ψ_c
4
5
6
7
8
9
10
11
12
T_e (eV)
B_p, V_e = 2.5 kv
t = INJ + 5msec
GUN INJECTION
AT 5 msec
IN PULSE (22°)
$p_o = 4.5 \times 10^{-7}$ TORR

The cooling mechanism is still experimentally not determined, although a hypothesis is presented in Chapter IV which might partially explain it.

It should be mentioned in passing that Navratil[5] has measured a different $T_e/\dot{T}_e$ using the admittance probe technique.[6] T_e was seen to drop with about a 20 msec decay time until it reached 1 eV. It stayed at that value for the remainder of his observation time. The transition time would occur after the observation time of Figures 3 and 4, which was chosen to be the time interval for levitation. The final resolution of this data conflict must await the acquisition of point for point data and its analysis using Strait's non-biased computer technique to avoid systematic error.

(ii) The Ion Temperature

Figure 6 of the ion temperature is included for completeness. This is a compilation of T_i measurements made by a number of observers using different techniques.[5,7,8] The results are summarized in Table I 2 for hydrogen. All T_i measurements were made in the B = 0 region of the octupole. However, $\nabla T_i = 0$ may be assumed due to the same processes used to explain the observed flat T_e profile.

B: Plasma Profiles

Figure 7 shows the ion saturation current and floating potential traces as a function of time for four positions across the lower outer bridge region at 330°. See Figure I 5 for the conversion from centimeters from the ring in the bridge to the corresponding ψ value. The data were obtained using the cleaned double platinum probe described in

Figure III 6

$T_i(t)$ from measurements by Breun ○, Navratil □, and Brouchous △. All data is acquired at the field null.

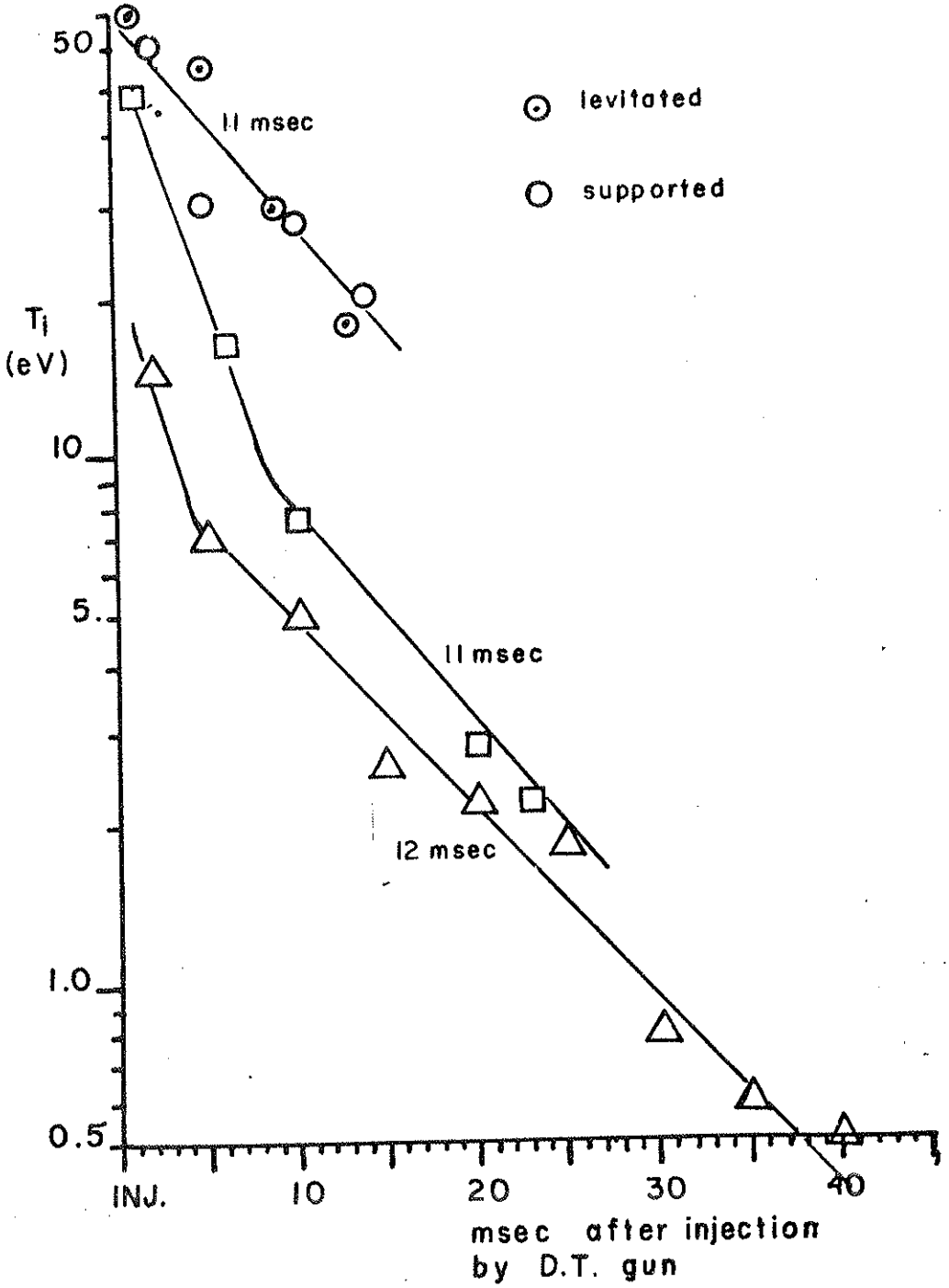
levitated
supported
11 msec
11 msec
12 msec
T_i (eV)
50
10
5.
1.0
0.5
INJ.
10
20
30
40
msec after injection by D.T. gun

Figure III 7

(A-D) $I_s(t)$ data traces at four positions in the bridge for the operating case of Figure 3. A, 1.75 cm; B, 4.5 cm; C, 7.0 cm; D, 8.0 cm.

(E-H) $V_f(t)$ traces for four positions in the lower outer bridge for the same plasma as in (A-D). E, 1.75 cm; F, 5.0 cm; G, 7.0 cm; H, 9.5 cm. Units per vertical division are marked on left of each base line as ABC YZ = ABC $\times 10^{YZ}$ amperes for I_s or volts for V.

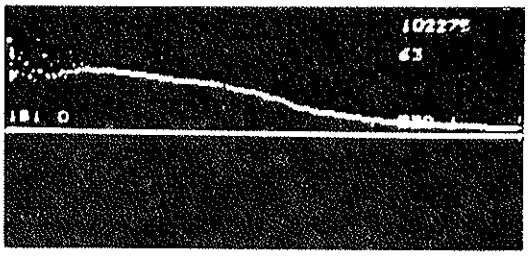
102278
63

A

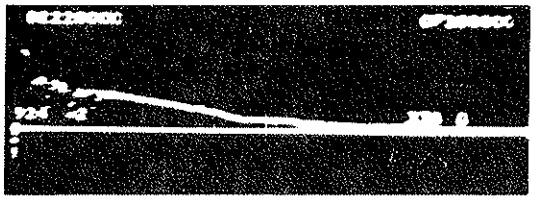

E

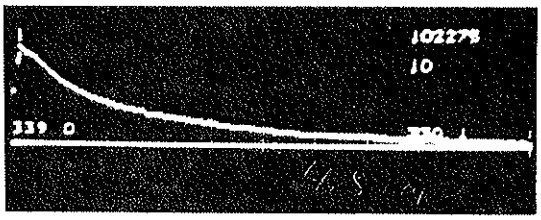
102278
10

B

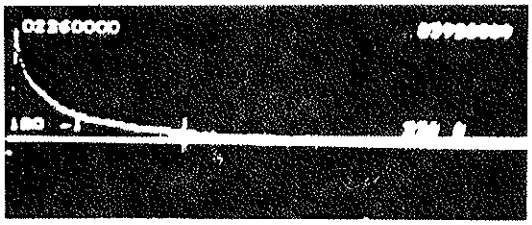
02260000

F

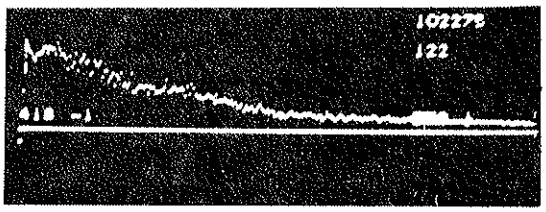
102278
122

C


02300000

G

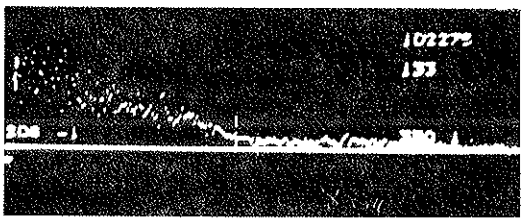
102278
133

D

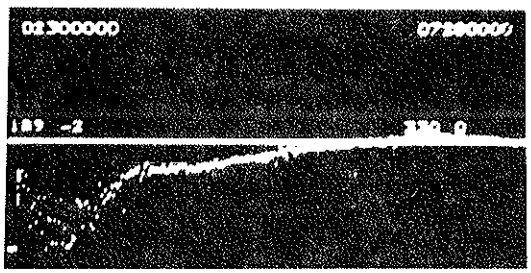
02300000

H

Chapter II. In these traces, as well as in all subsequent data, the ion saturation current are plotted in units of current density, μAmperes per square centimeter. Profiles for these data and others similar are presented in Figures 8 through 13. In each case, the profiles were acquired according to the prescription of II C. Four profiles, each at a different time, are presented for each of the six different machine configurations. The earliest time given for each set shows the plasma 1 msec after injection. Each time frame pairs the (upper) V_f profile, marked in volts of the peak value, with the (lower) ion current density, in μAmperes/cm^2 of its peak value. The particle densities corresponding to the ion current density may be estimated using [II-A-1]. All data were acquired with the clean double probe except the SINE case profiles, which were from single tipped gold probes cleaned as well as possible prior to insertion. The accuracy of these single tipped profiles is discussed in III E where the problems mentioned in II A are again examined.

Figure 14 is included to document the existence of what must be called an atypical profile. It is for the same machine parameters as Figure 9 but shows the profiles peaking on ψ_s with a relatively high I_s, a ∇I_s near the ring which points toward the ring, and a double humped V_f profile. This sort of profile has been seen on rare occasions by several other observers[9] since the gun was first installed. It is unknown what is responsible for this distribution, but it has usually been a transient state of the gun's operation which disappears after a day or so. These particular data, however, were observed after the extender on the gun (section I B) was removed and disappeared when the

Figure III 8

Poloidal field only, crowbarred case, supported rings. Profiles of floating potential (upper) in volts, and ion saturation current density (lower) in $\mu A/cm^2$ versus centimeters from the lower outer ring in the bridge at 330°. V_c = 2.5 kV, $P_o = 2 \times 10^{-7}$ Torr.

A. 23 msec, 1 msec after injection

B. 35 msec

C. 47 msec

D. 65 msec

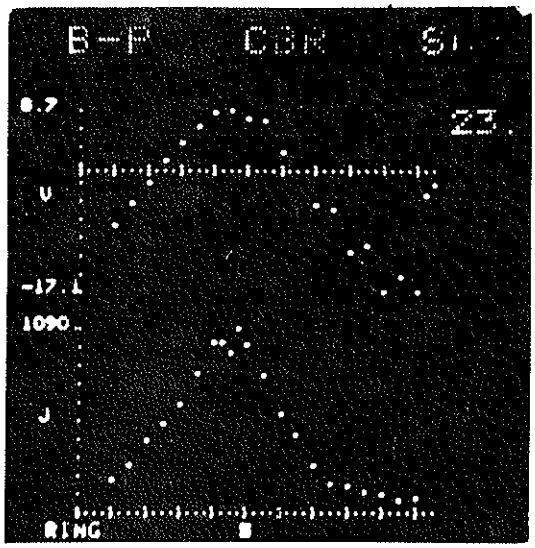
B-P
CBR
23.
V
J
RING

A

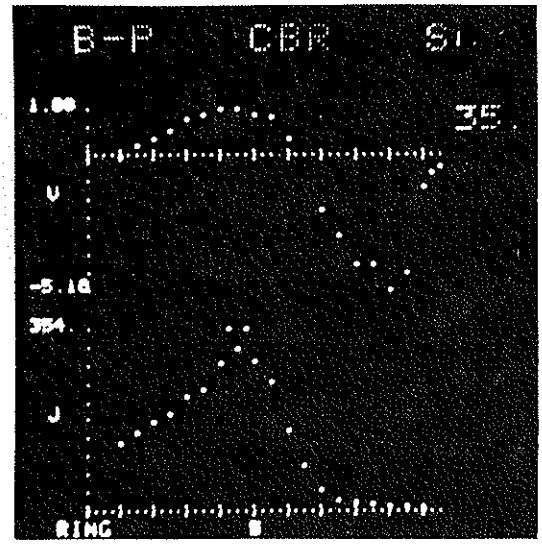
B-P
CBR
35.
V
J
RING

B

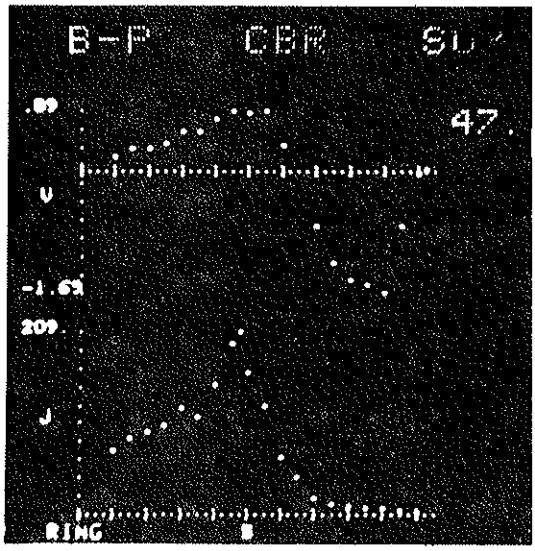
B-P
CBR
47.
V
J
RING

C

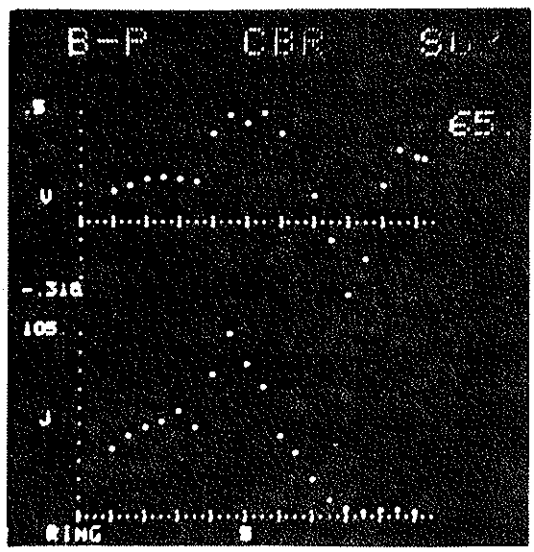
B-P
CBR
65.
V
J
RING

D

Figure III 14

Anomalous profiles. Operating conditions same as in Figure 8. Injection at 25 msec. The potential V is plotted in volts, the saturation current in μA.

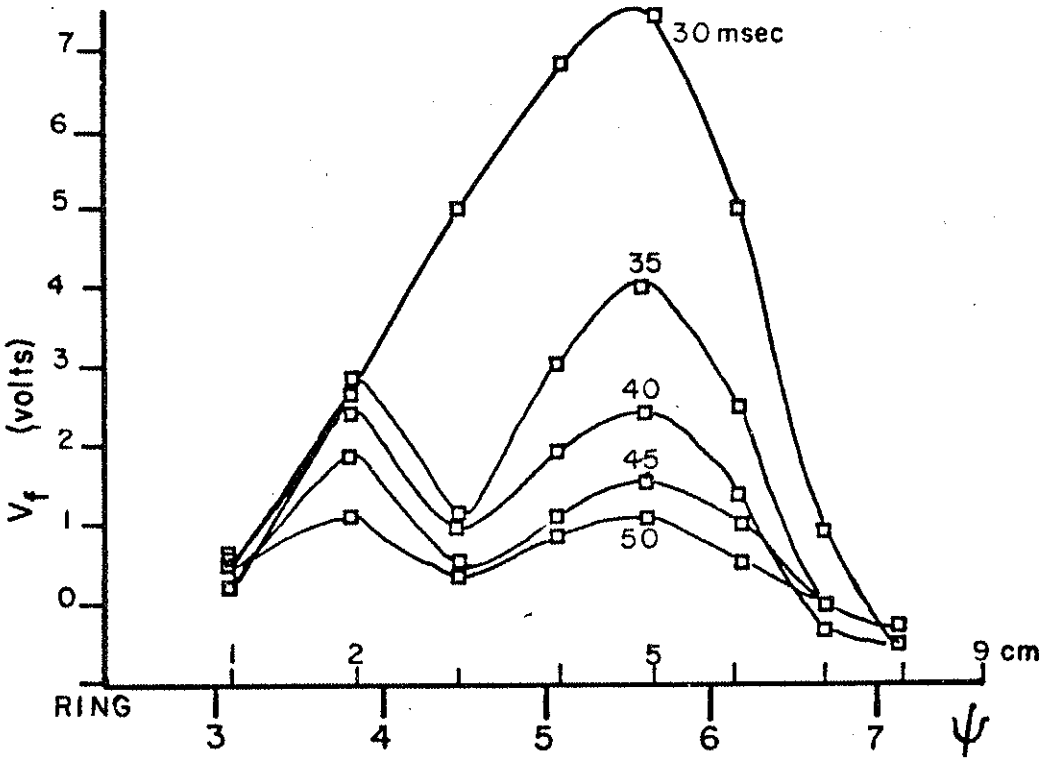
30 msec
35
40
45
50
V_f (volts)
0
1
2
3
4
5
6
7
1
2
5
9 cm
RING
3
4
5
6
7
ψ

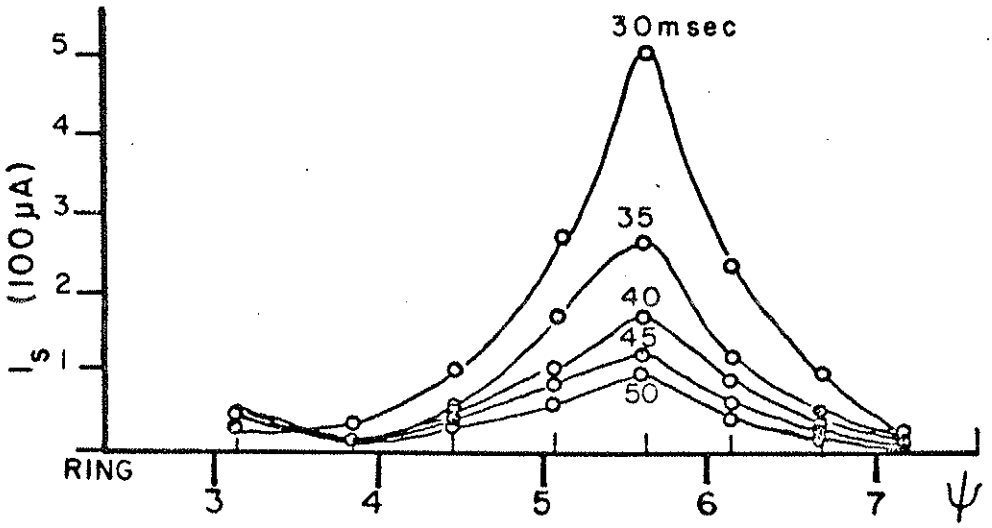
30 msec
35
40
45
50
I_s (100 μA)
1
2
3
4
5
RING
3
4
5
6
7
ψ

extender was replaced.

It should also be mentioned that the V_f profiles for the supported ring cases occasionally display an apparently arbitrary D.C. offset from the values shown here. The peak V_f value has actually been seen to be negative, but the potential gradients remain the same except at the walls and very close to the rings where the profile rapidly returns to ground potential. The offset does not appear to affect the density or any other parameter and, in fact, has been restorable to the "typical" value shown by levitating the rings.

Most of the "normal" profiles presented have two striking features in common. Firstly, the sign of ∇V_f implies that the electrons more readily leave the plasma than the ions. Secondly, V_f and I_s peak together in space. Since there are no gradients in temperature, [II-A-1 and 2] imply that the space potential and particle density do also. In addition, a linear relationship is observed between $\ln[I(x)]$ and $V_f(x)$. This is the topic of section D and was first suggested from the fluctuation phase velocity measurements as discussed in Chapter V.

A great deal has previously been discovered about the density profiles in the octupole with the poloidal field only. The magnitude and scaling of the ambipolar diffusion coefficient, $D_\perp$, (defined below) has been measured[10,11,12] and it has been shown that the density profile decays in a stable normal mode due to the diffusion driven particle flux.[13,14] It seems reasonable in this case to look for a diffusion explanation for the relation between $\underline{E} = -\nabla V_f$ and n.

Rudmin[15] has shown that late in the sine field case, the density distribution moves with the field lines in response to the behavior of

the machine's electric field. Hence a diffusion relation between n and V_f might be expected to fail late in the sine field cycle. In the case of the added toroidal field, the plasma has been seen to subdivide into regions where different processes dominate.[16] This should also confuse any overall pattern to the relationship between V and I.

C: The Ambipolar Density: Potential Relationship

Section III B shows that the probe saturation current and floating potential are related. This section gives a phenomenological explanation for this observed relationship. A kinetic theory model which quantitatively accounts for the data is presented in Chapter IV. The ambipolar assumption is that in every region in space the ion and electron densities increase or decrease at the same rate.[17] The continuity equation relates the particle fluxes, $\underline{\Gamma} = n\underline{v}$, for both species by

$$\nabla \cdot \underline{\Gamma}_i = \nabla \cdot \underline{\Gamma}_e \qquad \text{[III-C-1]}$$

The general solution of [1] is

$$\underline{\Gamma}_i = \underline{\Gamma}_e + \underline{\gamma} \qquad \text{[II-C-2]}$$

where the particle flow imbalance $\underline{\gamma}$ is the curl of some vector, $\underline{\gamma} = \nabla \times \underline{\beta}$. The vector $\underline{\beta}$ is related to the magnetic field caused by the net charge flow and must be determined by the boundary conditions of the problem. The flux coordinates of Chapter I will be used but the components of a vector parallel to $\underline{B}$ will be labeled with $||$. Since the octupole is azimuthally symmetric, $\Gamma_{i\zeta} = \Gamma_{e\zeta}$. It has been shown[18] that the average of $\underline{\gamma}$ around the closed field line is zero but local paral-

lel current imbalances may exist even with $E_{||} = 0$. The parallel and perpendicular components then must be left as

$$\Gamma_{i||} = \Gamma_{e||} + \gamma_{||} \qquad \text{[III-C-3a]}$$

$$\Gamma_{i\psi} = \Gamma_{e\psi} + \gamma_{\psi}. \qquad \text{[III-C-3b]}$$

Frequently the vector $\underline{\gamma}$ is arbitrarily set to zero. Although it has been shown that the average current ($e \langle\gamma\rangle$) crossing a closed field line is zero, the perpendicular current at any point on the field line may be a large value. The fact that $\underline{\gamma} = 0$ is not a justifiable relationship causes important problems with the interpretation of many types of data. This point is again discussed in section E.

For small displacements from thermodynamic equilibrium, the thermodynamic fluxes may be related linearly to the thermodynamic forces by the usual[19] Onsager expressions. The most general linear transport equation for the particle flux may be written as ($n_i = n_e = n$)

$$\underline{\Gamma}_e = -\nabla \cdot (\underline{\underline{D}}_e n) - n\underline{\underline{\mu}}_e \cdot \underline{E} \qquad \text{[III-C-4]}$$

$$\underline{\Gamma}_i = -\nabla \cdot (\underline{\underline{D}}_i n) + n\underline{\underline{\mu}}_i \cdot \underline{E} \qquad \text{[III-C-5]}$$

The subscripts are for ions and electrons and the equations are written so that the general coefficients $\underline{\underline{D}}$ and $\underline{\underline{\mu}}$ are identifiable as diffusion and mobility. $\underline{\underline{D}}$ and $\underline{\underline{\mu}}$ are written as second ranked tensors and the equations are structured as shown because these are the forms prescribed for a model dependent case by the fluid equations[20] or kinetic theory.[21] For the purpose of this paper, $\underline{\underline{D}}$ and $\underline{\underline{\mu}}$ will be considered

unrelated diagonal phenomenological transport parameters.

Rudmin[22] has used simple probe theory and has shown that, to within experimental accuracy, the observed plasma density in the octupole is constant along a field line, as expected by M.H.D. theory. As assumptions, let $E_{\|} = 0$ and all quantities be independent of ζ. Let the plasma potential be U so that $E = -\nabla U$, then [3], [4], and [5] yield (see Reference 18)

$$\frac{\partial U}{\partial \psi} = T^* \frac{1}{n} \frac{\partial n}{\partial \psi} + \frac{[\nabla \cdot (\underline{\underline{D}}_e - \underline{\underline{D}}_i)]_\psi - \gamma/n}{[\underline{\underline{\mu}}_e + \underline{\underline{\mu}}_i]_{\psi\psi}} \qquad \text{[III-C-6]}$$

where

$$T^* = \frac{[\underline{\underline{D}}_e - \underline{\underline{D}}_i]_{\psi\psi}}{[\underline{\underline{\mu}}_e + \underline{\underline{\mu}}_i]_{\psi\psi}} \qquad \text{[III-C-7]}$$

With [5] and [6] the electron flux becomes

$$\underline{\Gamma}_e = -D_a \nabla n + \underline{g}_e. \qquad \text{[III-C-8]}$$

The ambipolar diffusion coefficient D_a is

$$D_a = \frac{\mu_{e\psi\psi} D_{i\psi\psi} + \mu_{i\psi\psi} D_{e\psi\psi}}{\mu_{e\psi\psi} + \mu_{i\psi\psi}} \qquad \text{[III-C-9]}$$

and the flux imbalance is

$$\underline{g}_e = \frac{-\hat{\psi}}{\mu_{e\psi\psi} \mu_{i\psi\psi}} [\mu_{e\psi\psi}\gamma + n(\mu_{e\psi\psi} \nabla \cdot \underline{\underline{D}}_{i\psi} + \mu_{i\psi\psi} \nabla \cdot \underline{\underline{D}}_{e\psi})]. \qquad \text{[III-C-10]}$$

If T* is a constant in ψ, [6] may be integrated to yield

$$U(\psi) = U_o - T^* \ell n(n_o/n) + W(\psi) \qquad \text{[III-C-11]}$$

The subscript zero indicates the maximum value of U or n. As seen in Figures 8-13, these occur at the same place in space which indicates that the function $W(\psi)$ in [11] is a constant. W is the ψ integral of the term in [6] involving γ, which must be zero. This sets

$$\gamma = n\nabla \cdot (\underline{\underline{D}}_e - \underline{\underline{D}}_i)\Big|_\psi \qquad \text{[III-C-12]}$$

and also [10] will become

$$\underline{g}_e = -n(\nabla \cdot D_e)_\psi \, \hat{\psi}. \qquad \text{[III-C-13]}$$

Note that [11] need be true only in a piecewise fashion, between each region where the gradients go to zero. T* must be constant in each interval for [11] to be valid, but may change its value at the peaks.

D: Analysis Of The Profile Data

(i) Ambipolar Relation for V_f and I_s

The absence of temperature gradients for the profiles of III B imply that $V_f(\underline{x}) = V_p(\underline{x}) + a$ and $I_s(\underline{x}) = n(\underline{x})b$, where a and b are independent of position. This permits the conversion of [III-C-6] or [11] into a form with measurable parameters. As indicated, $W(\psi) = 0$ and ambipolar diffusion effects predict that

$$V_f(\psi) = V_o + T^* \ln[I_s(\psi)/I_o] \qquad \text{[III-D-1]}$$

where T* is still prescribed by [III-C-7] and V_o, I_o are the maximum value in ψ of V_f, and I_s. T* may be found from the slope of the plot of $\ln(I_s)$ v.s. V_f using the spatial coordinate as the common parameter to generate the (lnI,V) graph coordinates.

(ii) Parameterized (I,V) Plots

Figures 15-20 show the parameterized (I,V) plots of the profiles of Figures 8-13, respectively. There are four distinct regions visible in the plots for the B_p only cases. Regions I and II are in the closed field line portion of the octupole. Region I extends from near the rings to the mutual peak in density and potential. Region II extends from the peak to near the wall. As explained below [III-C-1], these represent good piecewise solutions of [III-C-6] in the form of [1]. Region III extends inward from the wall to a point where $\nabla V = 0$, where it becomes II. n does not go to zero at this place, but the $\nabla V = 0$ field line is the one which first terminates on the wall. (See Figure I 2.) Plasma in this region is mirror confined and $\Gamma_{i\|} = \Gamma_{e\|}$ is no longer necessarily true. III is external to the confinement zone and is characterized by a high level of fluctuations. Figure 21 shows the transition between regions II and III clearly for data taken along the mid cylinder where $d\psi/dx$ is small.

An example from a completely different plasma device is shown in Figure 22, which is the parameterized (I,V) graph of data from the D.C. spherator ring at Wisconsin taken with R. Richards using his marginally stable mirror configuration.[23] The plasma is mirror confined for this case and is shown for several values of bias on the single tipped probe used to acquire the data. T_i for this plasma is ten to a hundred times lower than T_e.

Region IV in the octupole plots begins at the ring and extends about an ion gyro diameter into the plasma, where it joins I. IV therefore corresponds to the ring scrape-off region.

Figure III 15

(I,V) graph of Figure 8. Heavy dots are data, light dots are the fitted curve to these dots. Abscissa marked in 0.5 V steps.

A. 23 msec

B. 35 msec

C. 47 msec

D. 65 msec. Short upper line is the ring-peak region I.